SECTION B. AREA OF REVIEW AND CORRECTIVE ACTION PLAN
40 CFR 146.84(b)

MONTEZUMA CARBON SEQUESTRATION HUB

Facility Information

Facility name: Montezuma Carbon Sequestration Hub
IW-1A

Facility contact: Jim Levine, Managing Partner
2000 Powell Street, Suite 920
Emeryville, CA 94608
Phone: (510) 409-1765
Email: jim.levine@upstream.us.com

Well location: Collinsville, Solano County, California
Lat: 38º5’7.334” N Long: -121º51’30.914” W NAVD 88
Sec 22 T 3 N R 1 E

Table of Contents

List of Tables

List of Figures

List of Appendices

B.1 PLANNED COMPUTATIONAL MODELING

B.1.1 MODEL NAME AND AUTHORS/INSTITUTION

TReactMech V4.213/ECO2N V2

The computational modeling for the MC project is being performed by a team of professionals associated with UC Berkeley/Lawrence Berkeley National Laboratory (UCB/LBNL).

B.1.2 DESCRIPTION OF MODEL

TReactMech is a parallel Thermal-Hydrological-Mechanical-Chemical (THMC) continuum geomechanics simulator based on TOUGHREACT V4.13 OMP (Sonnenthal et al., 2021; Xu et al. 2011), with improvements to the TOUGH2 (Pruess et al., 1999) multiphase flow core. The geomechanical formulation is based on a 3-D continuum finite-element model with full 3-D stress calculations, plastic deformation via shear and tensile failure (Kim et al., 2012; 2015; Smith et al., 2015; Sonnenthal et al., 2018). The equation of state (EOS) TOUGH reservoir simulation package ECO2N V2.0 (Pan et al., 2015; Pruess and Spycher, 2007; Spycher and Pruess, 2005) was used to model the CO_2 plume and pressure propagation into the earth. This package considers H_2O, NaCl, and supercritical CO_2 fluid flow and is multi-phase extension to Darcy's law, with inter-phase effects controlled by capillary pressure and relative permeability functions, which may be hysteretic (Doughty, 2007, 2013). Using the capability in ECO2N, solid NaCl salt, or more complex salt mineral assemblages may precipitate from solution (using the reactive-transport capabilities), with reversible changes in porosity, permeability, and capillary pressure.

TReactMech is ideally suited for continuum representations of fractured and porous rock masses at scales of meters to tens of kilometers (Sonnenthal et al., 2018). TReactMech can also simulate processes at the scale of individual fractures, such as for simulating hydraulic fracturing, or single-fracture deformation at the core-scale (Dobson et al., 2021). The continuum model approach considers local (grid-block scale) averaging of fracture porosities and permeabilities. Heat and fluid flow, stress, and reactive transport are solved using the sequential non-iterative approach. Fluid flow and heat transport are solved simultaneously as in TOUGH2 (Pruess et al., 2012) with modifications to consider multiple coupled geochemical and geomechanical effects on porosity and permeability. TReactMech uses a hybrid parallel computation approach, in which the geomechanics and fluid flow are solved using PetSc/MPI and the reactive chemistry with OpenMP. Geomechanics (3D stress equations, strain and failure strain) are solved after fluid and heat flow, followed by transport of aqueous and gaseous species, mineral-water-gas reactions, and finally permeability-porosity-capillary pressure changes owing to geomechanical and geochemical changes to porosity (or fracture aperture).

The TOUGH codes have been widely used over the past 20 years to study CCS, including scoping and design studies, code comparisons, and analysis of laboratory and field data (Doughty and Myer, 2009; Birkholzer et al., 2012; Pruess et al., 2004; Doughty et al., 2008; Finsterle et al., 2014; Aradóttir et al., 2012).

Geochemical reactions are not considered in the simulations presented in this report. All multiphase simulations are non-isothermal and consider gradients in salinity coupled to density and viscosity, and salt precipitation during dryout.

B.1.3 MODEL INPUTS AND ASSUMPTIONS

The geologic/hydrogeologic information that serves as inputs to the model are summarized in the following subsections and described in more detail in the Section A.I Site Characterization portion of the application.

Regional Geology, Hydrogeology and Local Structural Geology

The proposed injection site is in southwestern Montezuma hills, an area of modestly elevated topography north of the Sacramento River between the reclaimed Delta islands to the east and southeast, and Grizzly Island and Suisun Bay to the west (Figure B-1). The Montezuma hills are at the southwestern end of the Sacramento Valley, a subaerial, intermontane basin between the Coast Ranges to the west and Sierra Nevada to the east. The modern Sacramento Valley evolved from an ancestral Mesozoic-Tertiary marine forearc basin that formed above a long-lived, east-dipping subduction zone beneath western California (Ingersoll and Dickinson, 1981). Over the past approximately 28 million years, plate convergence and subduction have been progressively replaced by transcurrent motion and strike-slip faulting in western California, leading to shoaling of the marine basin, uplift of the Coast Ranges to the west, and a transition to continental fluvial deposition in the Sacramento Valley (Graham et al., 1983, and references therein).

The Montezuma hills approximately coincide with the central part of Rio Vista basin, a north-south-trending extensional sub-basin within the larger forearc basin that formed in early Tertiary time (MacKevett 1992; Krug et al. 1992). Although the early Tertiary Rio Vista basin is now buried north of the Sacramento River by younger Tertiary and Quaternary terrestrial deposits, an oblique cross-sectional view of the bounding structures and thickened Paleogene marine section in the basin is exposed south of the river in the northeast-dipping backlimb of Mount Diablo anticline. From inspection of this natural, map-scale cross section, the Midland and Kirby Hills fault zones form the eastern and western margins, respectively, of the Rio Vista basin (Figures B-1 and B-2). Both structures were originally normal faults, and they can be traced in the subsurface of Rio Vista basin southward across the river into the exposed stratigraphic section on the northern flank of Mt. Diablo. The structure correlative to the Kirby Hills fault south of the river is the Kirker fault, which is exposed in the Los Medanos hills between the cities of Pittsburg and Concord.

Secondary normal faults splay west-northwest from the Midland fault and terminate westward against the Kirby Hills fault zone (Krug et al., 1992), forming local structural lows within the larger Rio Vista basin. Examples of these secondary structures include: the Sherman Island fault, which is known from exploration and development of the Sherman Island gas field; and the Antioch and Davis faults, which are mapped in Tertiary outcrops south of the river. The Sherman Island fault is mapped west of and subparallel to the Midland fault, and interpreted to dip moderately to steeply east, antithetic to the Midland fault (DOGGR, 1982b). Krug et al. (1992) map other east- to northeast-dipping secondary normal faults beneath the central Montezuma hills between the Midland and Kirby Hills faults.

FIGURE B-1. MAP OF MAJOR FAULTS IN THE MONTEZUMA HILLS STUDY AREA.

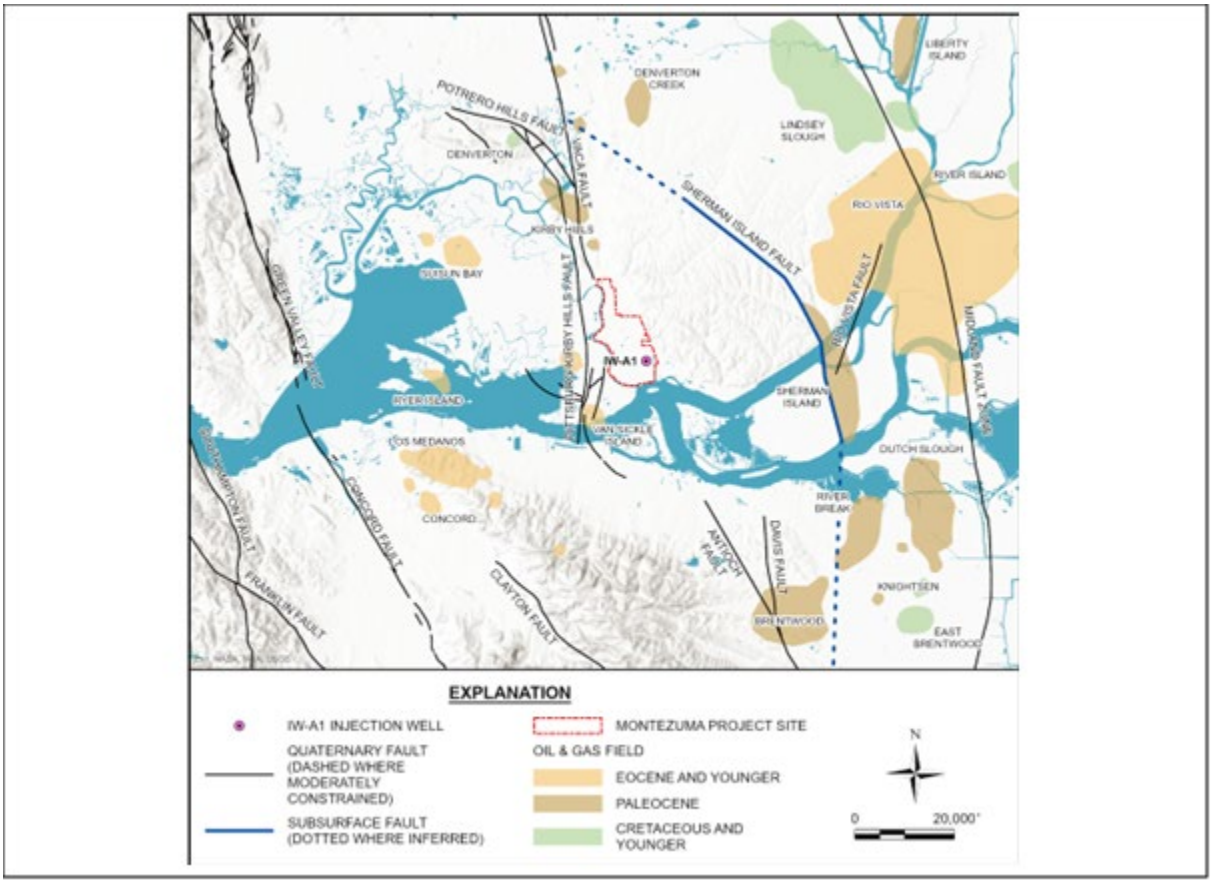

FIGURE B-2. CROSS-SECTION OF THE MONTEZUMA HILLS STUDY AREA

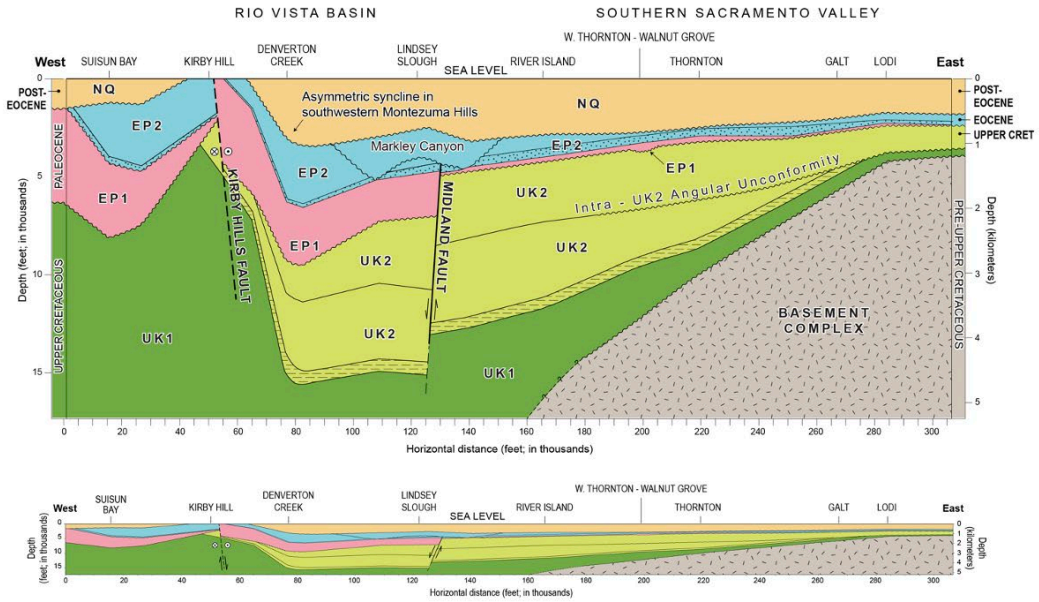

Simulation Model Domain

The reservoir model was represented by a 146 × 146 × 148 grid in a Cartesian system with 146 grid points in the x-direction, 146 grid points in the y-direction, and 148 grid points in the z-direction, for a total of 3,154,768 grid points. Model domain information is summarized in Table B-1.

TABLE B-1. MODEL DOMAIN INFORMATION

Coordinate System	State Plane		
Horizontal Datum	NAD27		
Coordinate System Units	ft		
Zone	SPCS27-1201		
FIPSZONE	1,201	**ADSZONE**	3,776
Coordinate of xmin	277,028.18	**Coordinate of xmax**	408,692.78
Coordinate of ymin	1,103,729.25	**Coordinate of ymax**	1,235,364.89
Coordinate of zmin	-7113.19	**Coordinate of zmax**	-4272.78

Model Geometry

The model dimensions were 6 km E/W by 18 km N/S with the injection well located in the center of the model. No-flow boundaries are applied at all model boundaries, except at the top of the full model, which

represents the atmosphere. The 6 km E/W distance was selected to create a no-flow boundary at the projected distance between Kirby Hills Fault at the Anderson level and the injection well. As described in the Site Characterization of this permit, the Kirby Hills Fault traps gas on the east side of the fault and possesses sealing upper Cretaceous shales on the west side of the fault. The grid resolution is variable, with finest resolution around the injection well (25 m). The figure below shows a cut-away view of the model, illustrating the gridding. The Anderson reservoir was 396.3 m thick, with 16 layers, each 24.77 m. The lateral grid resolution at the injection well is 25 m. Examples of the 3-D grid (with cut-way), rock units, and permeability with a CO_2 plume at various times are shown in Figure B-3.

FIGURE B-3. EXAMPLES OF 3-D RESERVOIR MODEL GRID (TOP) AND PERMEABILITIES (BOTTOM) SUPERIMPOSED CO_2 PLUME AT 30 AND 40 YEARS

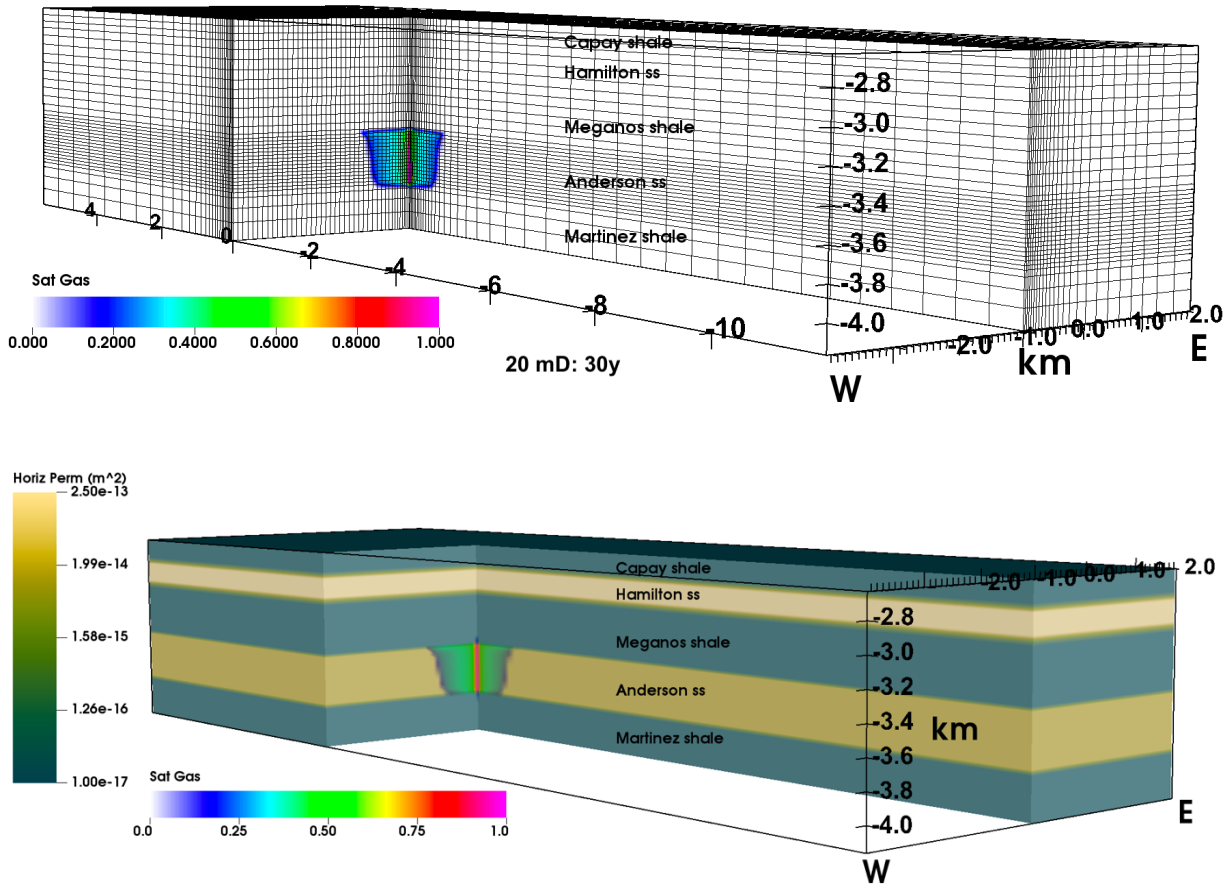

Reservoir Initial Conditions

An initial hydrostatic pressure gradient, geothermal temperature gradient, and given salinity gradient are specified for a 1D column model extracted from the full model, and the model is allowed to come to steady-state (1 million years). Pressure, temperature, and salinity are fixed at the top of the model (the ground

surface), and temperature is fixed at the base of the model. The temperature difference between model top and bottom corresponds to a geothermal gradient of 22.7 ºC/km. The initial salinity gradient is 3350 ppm/km, which was estimated from local literature values. Initial dissolved CO_2 concentrations were assumed to be uniformly 100 ppm. The 1-D steady-state temperature, pressure, salinity, and dissolved CO_2 profiles were used as initial conditions for the 3-D reservoir models. The 3-D models were then run for 10,000 years to a new steady-state to account for any local convective (thermo-haline circulation) effects.

Initial conditions at the top of the Anderson reservoir were as follows:

- Top of Reservoir: 3456.6 m
- Reservoir Temperature: 96.46 ºC
- Reservoir pressure 33.82 MPa
- Reservoir salinity 16,658 ppm
- Fluid density 987.27 kg/m^3
- Permeability (20mD, and a second run at 200 mD)
- Porosity 20%

Hydrological and Thermal Parameters - Hydrological and thermal properties are given for the 3-D reservoir model in Table B-2. Porosities and permeabilities are estimates from (Unruh et al. 2016). Unsaturated hydrologic properties (capillary pressure and relative permeability) for the van Genuchten (Pcap) and van Genuchten-Corey models are generic values for sandstones and shales. Thermal conductivities (bulk, kT) and grain heat capacities (Cp) are also generic values for sandstones and shales. Note that the permeabilities of the units were given anisotropy ratios (vertical/horizontal) of 0.1 for shales and 0.2 for sandstones to account for internal layering and heterogeneity not considered directly.

TABLE B-2. HYDROLOGICAL AND THERMAL PROPERTIES FOR THE 3-D RESERVOIR MODEL.

Rock	*kh,kv* (mD)	ϕ	K-rel	λ	S_{lr}	S_{ls}	S_{gr}	Pc ap	λ	S_{lr}	$1/P_0$ Pa^{-1}	k_T (w, d) $W\ m^{-1}\ K^{-1}$	Cp $J\ kg^{-1}\ C^{-1}$
Capay shale	0.01 0.001	0.20	VG-C	0.412	0.2	1.	0.05	VG	0.412	0.0	$5.32x10^{-5}$	2.0, 1.5	900.
Hamilton sandstone	250 50	0.19	VG-C	0.400	0.2	1.	0.05	VG	0.400	0.2	$2.79x10^{-4}$	2.5, 1.875	900.
Meganos shale	0.01 0.001	0.20	VG-C	0.412	0.2	1.	0.05	VG	0.412	0.0	$5.32x10^{-5}$	2.0, 1.5	900.
Anderson sandstone	20, 200 4, 40	0.20	VG-C	0.400	0.2	1.	0.05	VG	0.400	0.2	$2.79x10^{-4}$	2.5, 1.875	900.
Martinez shale	0.01 0.001	0.15	VG-C	0.400	0.2	1.	0.05	VG	0.400	0.0	$5.32x10^{-5}$	2.0, 1.5	900.

VG: Van-Genuchten
VG-C van Genuchten-Corey
kT (w,d) wet, dry thermal conductivities

Injection Conditions

Injection of 1 Mt/year gas at mass fractions of 98% CO_2 and 2% H2O was spread over the 16 intervals in the Anderson sandstone. An approximate enthalpy of CO_2 at 90°C and 20 MPa ($4.02x10^5$ J/kg) was derived from https://www.ohio.edu/mechanical/thermo/property_tables/CO2/C02_Transcrit2.html. The enthalpy of H_2O at 90°C and $1.01325x10^5$ Pa ($3.7696x10^5$ J/kg) was derived from https://www.thermexcel.com/english/tables/eau_atm.htm.

Simulation Parameters

The 3-D 20 mD reservoir simulation was run for 40 years of injection and then 60 additional years without any injection for a total of 100 years. A more permeable case with the Anderson sandstone set to 200 mD was run to 30 years injection. Timestepping in the simulations is dynamic and typically ranged from a few hours to several days.

Operational Information

The injection well is modeled as a column of 16 equal-thickness (24.77 m) grid blocks in the Anderson sandstone with areal extent 25 m by 25 m. The total amount of CO_2 injected (1 million tonnes per year) is divided equally among the grid blocks as mass sources with enthalpy approximately equal to the temperature of the grid block into which it is being injected. The Peaceman (1977) correction is applied to convert the grid-block pressure response to the response at a well with radius 0.3 m. This conversion is only needed for

verifying that the maximum operating pressure (determined below) is not exceeded. Table B-3 summarizes the operating details for the modeled injection.

TABLE B-3. OPERATING DETAILS FOR THE MODELED INJECTION WELL

Parameters and units		
Model coordinates (ft; m)	X	0
	Y	0
Injection Interval (ft; m)		11,300 to 12,600 ft; 3445 to 3840 m
Wellbore diameter at injection interval (in, m)		11.8; 0.3
Lateral extent of grid block containing well (m)		25
Peaceman (1977) correction for P (psi; MPa) (for 20 mD case)		20.3 psi; 0.14 MPa
Injection duration (years)		40
Injection rate (MMT/year)		1.0
Fracture gradient (psi/ft; kPa/m)		0.71; 16.02
Max. op. pressure (MOP) (psi; MPa)		7202; 49.7
Pressure Differential (MOP-Reservoir Pressure) (psi; MPa)		2291; 15.8

We chose 0.71 psi/ft = 16.02 kPa/m as the fracture gradient for the simulations, based on best estimates from local information. Table B-3 summarizes the Maximum Operating Pressure (MOP) based on this fracture gradient and a 90% safety factor. MOP is 49.7 MPa, thus, using the initial reservoir pressure estimate of 33.8 MPa, the maximum injection pressure is 15.8 MPa. This assumes a normally pressured reservoir. Recent analyses of mud weights on nearby wells suggest that the reservoir pressure may be underestimated by 10-20%, which would reduce maximum injection pressure to around 1000 psi or 8 MPa. Using a permeability of 20 mD, a net sand thickness of 910 ft, and an injectivity index of 0.08, yields an estimated maximum CO_2 injection volume into the Anderson of 1.4 MMtonnes/yr (Valluri, et al., 2021), which provides about 50% more injectivity than is planned.

B.2.2 THERMAL-HYDROLOGICAL-MECHANICAL MODEL

A preliminary analysis of the geomechanical response to CO_2 injection was performed using the initial and final 40 year pressure and temperature distributions from the 20 mD simulation, then solving the resultant 3D stress and thermo-poroelastic strain equations using TReactMech. Fracture generation was not allowed to take place by increasing the cohesion to a large value.

Geomechanical Properties and Boundary Conditions

Geomechanics controls the changes in stress and the potential for fracture generation or stimulation in response to pressure, temperature, and stress changes. In short, in response to changes δP, δT in pressure and temperature, and possible changes in strain δε, and stress δσ changes as

$$\delta\sigma = \mathbf{C}\,\delta\epsilon - \alpha_b \mathbf{I}\,\delta P - 3\,\alpha_{th} K_{dr}\delta T \qquad \text{Eq. 1}$$

where **C** is the stiffness matrix, α_b the Biot coefficient, α_{th} the coefficient of (lineal) thermal expansion, K_{dr} is the drained bulk modulus, and **I** is an identity matrix, where changes in possible failure strain δ ε) have been (temporarily) neglected. (Here we use a compressive stress negative convention.) Change in strain δ ε is found from the requirement that stress satisfy the force balance equation

$$\boldsymbol{\nabla \cdot \sigma} + \boldsymbol{\rho_b} = \mathbf{0} \qquad \text{Eq. 2}$$

Shear failure occurs if

$$\mathrm{F_{ij}} \equiv \boldsymbol{\sigma}_{\mathbf{ii}}^{(\mathbf{pr})}) - \sigma_{jj}^{(pr)} - 2\,C_{sh}\cos\phi_{fr} \quad + \left(\sigma_{ii}^{(pr)} + \sigma_{jj}^{(pr)}\right)\sin\phi_{fr} > \mathbf{0} \qquad \text{Eq. 3}$$

where $\sigma_{11}^{(pr)}$, $\sigma_{22}^{(pr)}\sigma_{33}^{(pr)}$ are principal effective stresses (effective stress components in coordinates in which stress is diagonal), C_{sh} is rock cohesion, and ϕ_{fr} is rock internal friction angle. Tensile failure occurs when the minimum effective exceeds the tensile strength.

We model equations (1-3) for δP, δT from the solution to the multiphase flow. Changes in stress σ, result in (thermoporoelastic) changes in porosity. In general, we model the problem of coupled flow and mechanics with changes in temperature and pressure affecting the mechanics and changes in porosity affecting the flow. However, due to time constraints, in the current work, the coupling of mechanics back to flow was approximated with a pore compressibility term based on rock bulk modulus and changes in pressure; changes

in stress and possible material failure were computed from the changes in pressure and temperature without coupling of mechanic back to flow beyond the pore compressibility term.

Bulk moduli under undrained conditions and shear moduli were computed from a model of P wave velocity (Vp) and S wave velocities (Vs) for the West (Sacramento) Delta region (Brocher, 2004), with density computed from a correlation with Vp (loc. cit.). Bulk moduli were adjusted to drained conditions using Gassman's equation, using the porosities in Table B-2, and estimated grain bulk moduli for sandstones and shales. Sandstones were assumed to have a grain bulk modulus of quartz (37 GPa). Grain bulk moduli for shales were computed for a 'typical' composition of 58 % clay minerals, 28 % quartz, 6 % feldspar, 5 % carbonates, 2 % iron oxides, with clay minerals portioned as 25% illite, 20 % kaolinite, and 14 % smectite, and feldspar treated as plagioclase. The structurally similar biotite bulk modulus was used for the (unmeasured) illite bulk modulus, following Asaka et al. (2021). Average bulk moduli of harder minerals and of softer minerals (kaolinite and smectite) were computed separately using volumetric reciprocal averaging, and the two averages combined treating the harder mineral component as matrix in an upper Hashin-Strikman bound average, yielding a 44 GPa estimated shale grain bulk modulus. The resulting elastic moduli under drained conditions are given in Table B-4, as well as Biot coefficients, computed from

$$\alpha_b \equiv 1 - K_{dr} / K_{gr} \qquad \text{Eq. 4}$$

where K_{dr} is drained bulk modulus, and K_{gr} is grain bulk modulus. Material cohesion, and internal friction angles were computed from Vp using correlations estimated for shales and said to also be fairly satisfactory for sandstones (Lai, 1999).

TABLE B-4. GEOMECHANICAL PROPERTIES

Unit	Bulk Modulus (GPa)	Young's Modulus (GPa)	Shear Modulus (GPa)	Poisson's Ratio	Biot coef	Friction Angle (deg)	Cohesion (MPa)	Tensile Strength (MPa)	Thermal Expansion Coef (1/°C)
Capay sh	17.5	28.2	11.4	0.232	0.603	36.0	7.3	7.3	1.0×10^{-5}
Hamilton ss	19.8	31.2	12.6	0.238	0.463	36.8	7.5	7.5	1.0×10^{-5}
Meganos sh	21.2	35.6	14.6	0.221	0.518	37.8	7.8	7.8	1.0×10^{-5}
Anderson ss	25.2	42.2	17.3	0.221	0.352	39.2	8.1	8.1	1.0×10^{-5}
Martinez sh	27.0	47.5	19.7	0.207	0.386	40.2	8.5	8.5	1.0×10^{-5}

Initial vertical stresses σ_{zz} were given by vertical loading stress, smoothed laterally. Initial horizontal stresses were set to $\sigma_{hmin} = 1.2\ \sigma_{zz}$, $\sigma_{Hmax} = 1.8\ \sigma_{zz}$, following Foxall et al. (2017). The maximum horizontal stress direction was approximated as North-South, and minimum as East-West. The upper model boundary (top of

Capay shale) was given a vertical traction for loading stresses computed for layers above it (57.555 MPa), sides given no normal displacement conditions, allowing upwards and lateral movement, and the lower model boundary no normal displacement conditions.

Boundary Conditions

No-flow boundaries are applied at all sides and the bottom model boundaries. The top layer of the full 3-D model represents the atmosphere as a constant-pressure, constant-temperature boundary. For the 3-D reservoir model the top of the Capay shale is treated as hydrostatic (fixed pressure and temperature) with values based on a 1-D steady-state simulation. The lateral boundaries of both the full and reservoir-only model are the same and are as follows:

West: Kirby Hills Fault
East and North: Sherman Island Fault
South: termination of Anderson Formation

Local information about pressures on opposite sides of the faults suggests that they are closed to flow. The bottom of the full model represents the granitic basement and is assumed to be closed. The reservoir-only model has an open upper boundary and a closed lower boundary to represent the top of the upper sealing layer and the bottom of the lower sealing layer of the storage reservoir, respectively. Although the top of the Capay shale is an open boundary, the vertical permeability of the Capay is set to 0.001 mD, so it is essentially impermeable.

B.3 COMPUTATIONAL MODELING RESULTS

B.3.1 CO_2 PLUME MODEL RESULTS

Results are shown as contour plots for W-E, S-N, and plan view (top of Anderson sandstone) sections at multiple time intervals in Figures B-3 to B-7. The radius of the CO_2 plume, shown as gas saturation in Figures B-3 through B-5, is about 1 km after 40 years injection, and 1.3 km after 100 years.

FIGURE B-3. CO_2 PLUME (GAS SATURATION) W-E CROSS-SECTION FOR 20 MD CASE AT 1, 20, 40, AND 100 YEARS

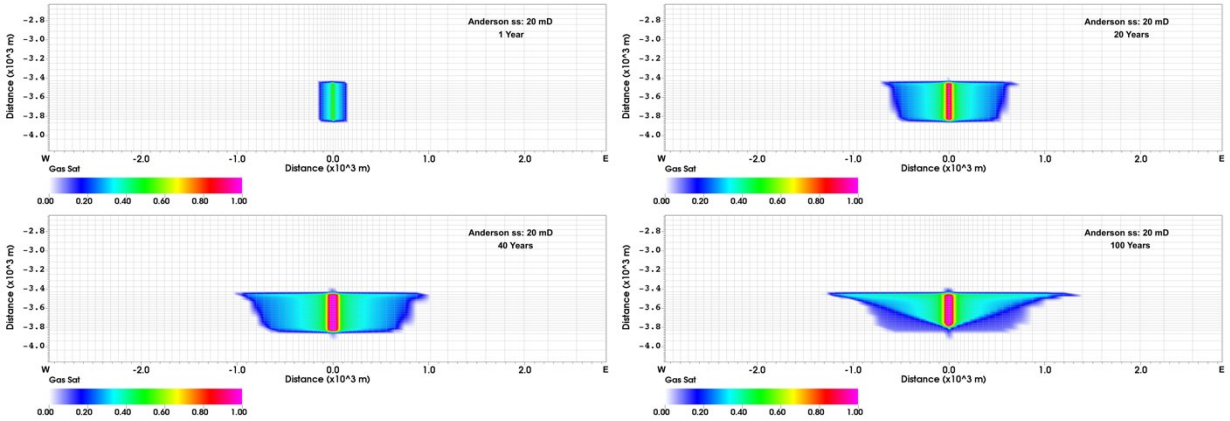

FIGURE B-4. CO_2 PLUME (GAS SATURATION) S-N CROSS-SECTION FOR 20 MD CASE AT 1, 20, 40, AND 100 YEARS

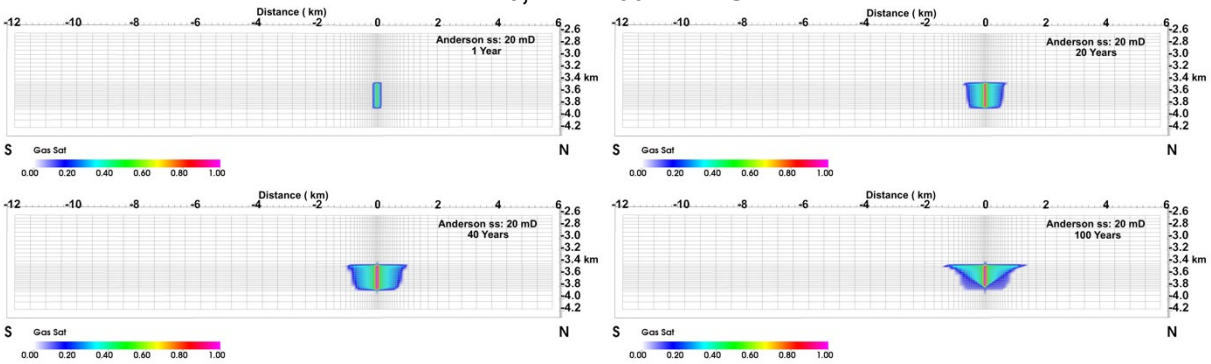

FIGURE B-5. CO_2 PLUME (GAS SATURATION) AT RESERVOIR TOP FOR 20 MD CASE AT 1, 20, 40, AND 100 YEARS

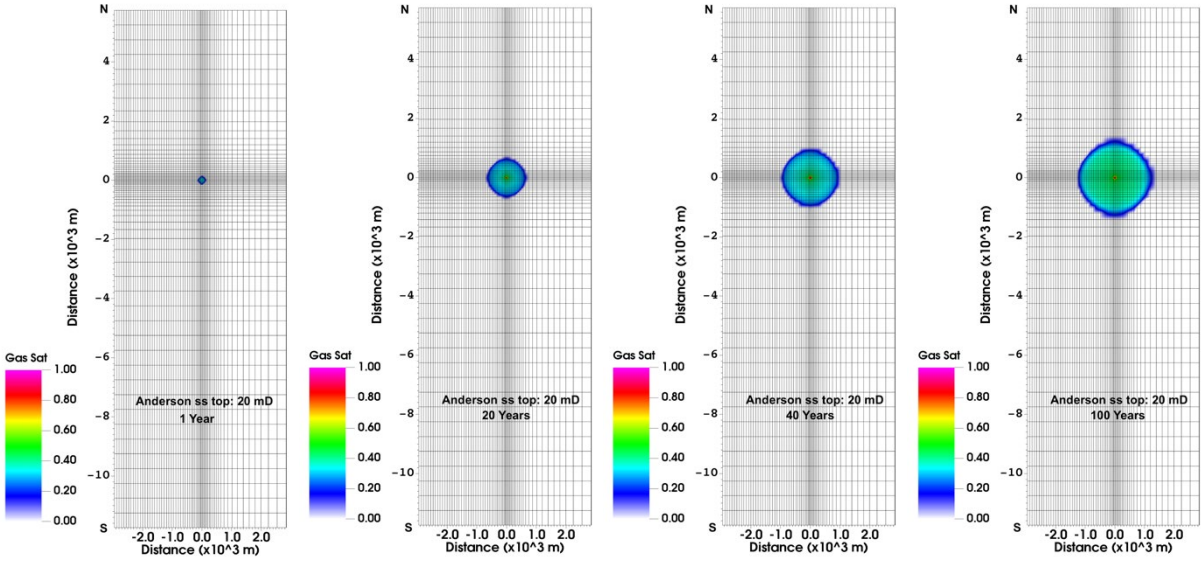

Pressure changes ($P\text{-}P_{hydrostatic}$), shown in Figures B-6 through B-8, show impacts at all boundaries early in the injection period with a maximum at the Kirby Hills Fault of about 1.6 MPa (20 mD case) after 40 years injection. Assuming a permeability of 200 mD leads to pressure increases of 1 MPa at the Kirby Hills Fault after 40 years injection.

FIGURE B-6. NONHYDROSTATIC PRESSURE W-E CROSS-SECTION FOR 20 MD CASE AT 1, 20, 40, AND 100 YEARS

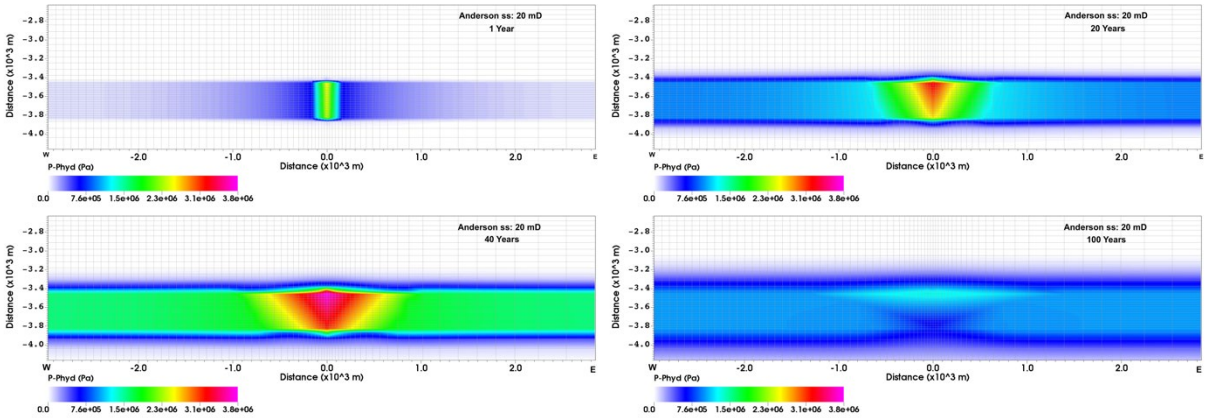

FIGURE B-7. NONHYDROSTATIC PRESSURE AT RESERVOIR TOP FOR 20 MD CASE AT 1, 20, 40, AND 100 YEARS

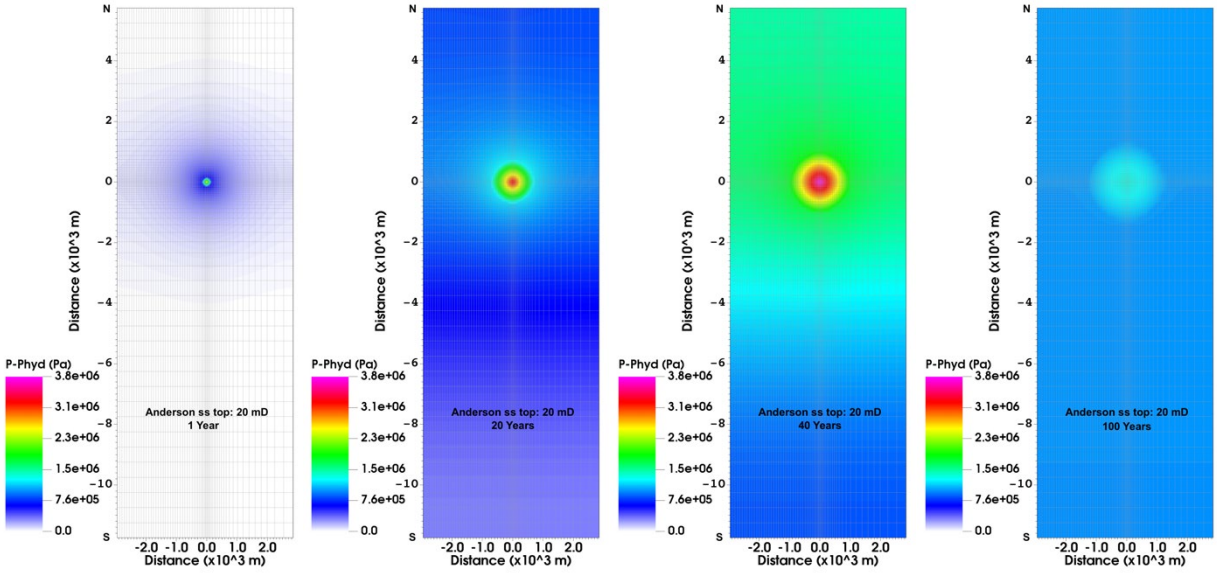

FIGURE B-8. NONHYDROSTATIC PRESSURE W-E AND S-N PROFILES AT RESERVOIR TOP: 20 MD (30 & 40 YEARS) AND 200 MD (30 YEARS)

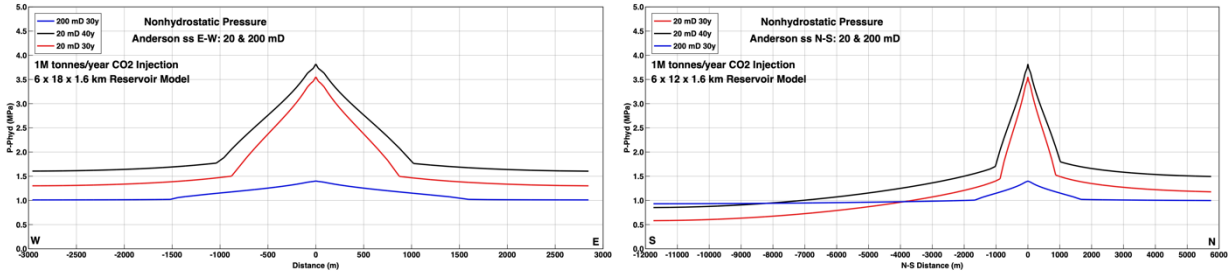

Pressure changes ($P\text{-}P_{hydrostatic}$), shown in Figure B-9, show impacts at the injection well IW-A1 that decrease substantially after injection stops, but remain elevated above background conditions, in the structurally (sealed fault) controlled setting for over 85 years after injection (125 years total).

FIGURE B-9. LONG-TERM PRESSURE CHANGE AT IW-A1 FOR 20 MD CASE AT 125 YEARS

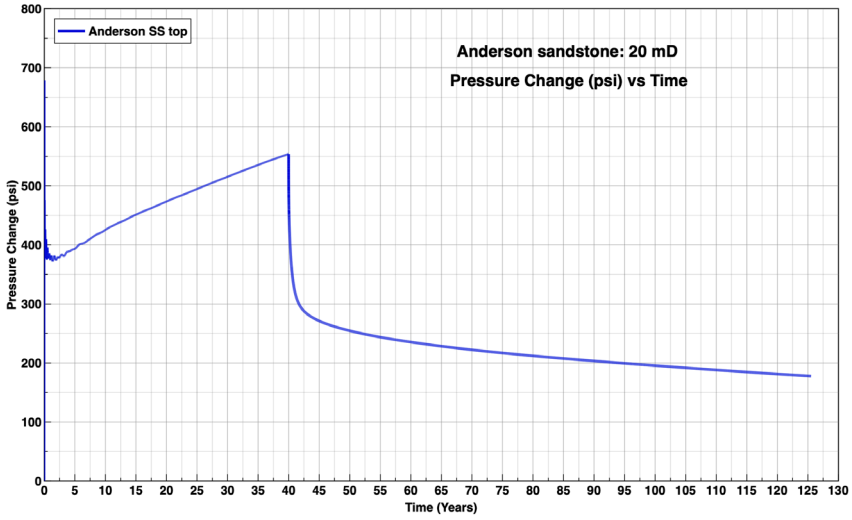

High concentrations of dissolved CO_2 (Figure B-10) extend only about 100 m further than the CO_2 plume after 100 years, and much less at 40 years.

FIGURE B-10. DISSOLVED CO_2 (MASS FRACTION) IN LIQUID SHOWN AT 40 AND 100 YEARS FOR THE 20 MD CASE

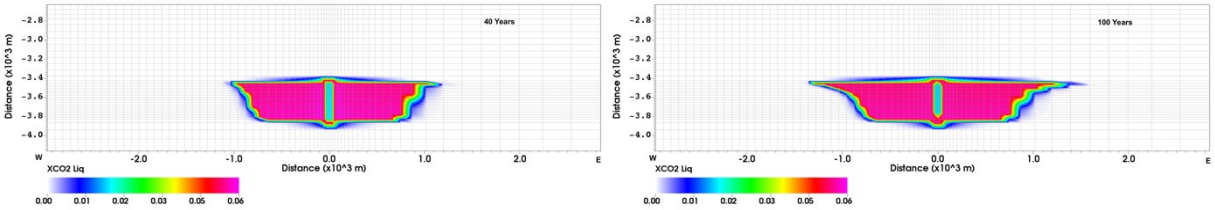

B.3.2 GEOMECHANICAL MODEL RESULTS

The approach used involved calculating the stress changes using the 40 year and initial injection pressures and temperatures (as described above), rather than running the fully coupled simulation for the full time. This method allows for a faster analysis of stress changes, while ignoring potential shear/tensile failure, and other simplifications described above, that may take place during injection.

Profiles of the stress changes for the primary directions from west to east are shown in Figure B-11. Two values of the Biot coefficient for the Anderson sandstone were used, 0.352 (Table B-4) and 0.8 (a conservative value similar to literature values for many sandstones). The higher the Biot coefficient, the higher the stress transferred to the fault, and therefore without site-specific data, a high and low value were considered. The plot shows the stress changes as generally positive (compressive). Although TReactMech by convention considers compressive stress as negative, the positive stress change with increasing fluid pressure is more intuitive and is plotted that way here.

FIGURE B-11. PROFILES OF THE STRESS CHANGES FOR THE PRIMARY STRESS COMPONENTS FROM WEST TO EAST AT 40 YEARS FOR THE 20 MD CASE

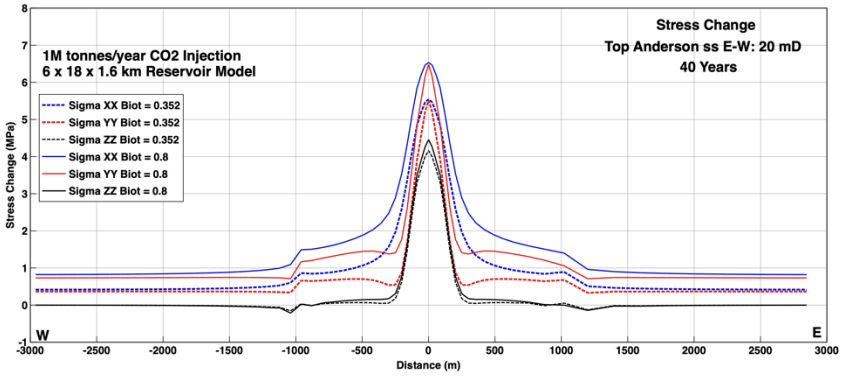

The greatest stress changes are evident at the plume center (~ 6.5 MPa) with up to about an 0.8 MPa increases at the west and east boundaries (σ_{xx}) for Biot coefficient equal to 0.8. Prior to injection σ_{xx} was the intermediate stress and minimum value in the horizontal plane (SHmin).

Cross-sections of the stress contours are shown in Figure B-12. The contour plots are directly from the code output for which compressive stresses are by convention negative, hence the plots show primarily negative stresses. Horizontal stresses (σ_{xx}) show the increased stress confined to the Anderson sandstone. Vertical stress changes (σ_{zz}) propagate a few hundred meters above and below the Anderson sandstone but are confined laterally to the plume region.

FIGURE B-12. CONTOURS OF STRESS CHANGES FOR THE PRIMARY COMPONENTS (DELTA σ_{xx}, DELTA σ_{zz}) FROM WEST TO EAST AT 40 YEARS FOR THE 20 MD CASE

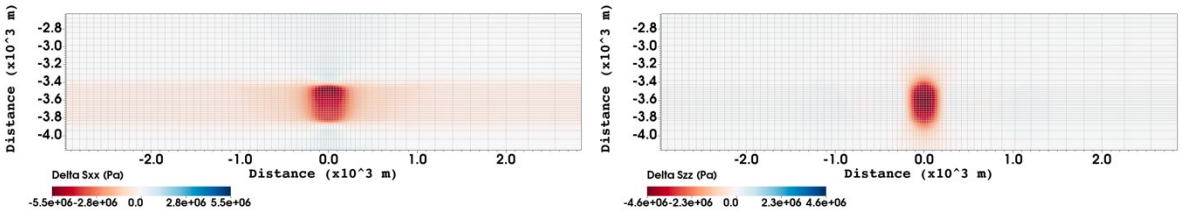

Plan views of the stress contours at the top of the Anderson sandstone are shown in Figure B-13. Over the 40 year period, the stress changes are generally similar in shape to the plume, with some stretching in W-E direction of the σ_{xx} stresses owing to the closer location of the boundaries (faults) and the asymmetric initial stress conditions.

FIGURE B-13. PLAN VIEWS OF STRESS CHANGE (DELTA σ_{xx}, DELTA σ_{zz}) CONTOURS AT THE TOP OF THE ANDERSON SANDSTONE

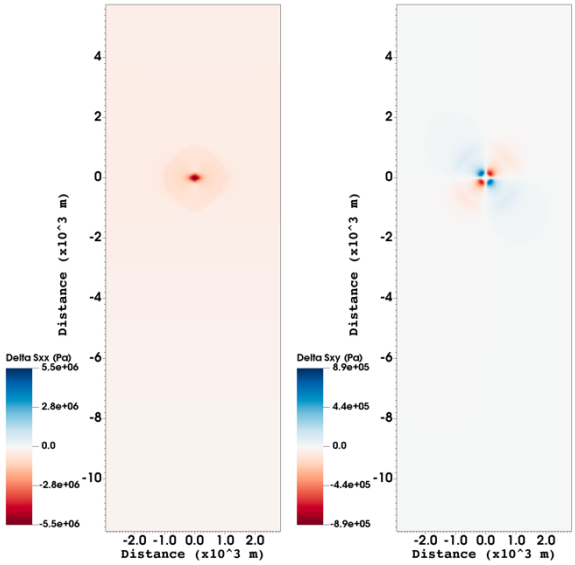

Future work - As improved information becomes available from site characterization and reservoir monitoring data, updated simulations will be performed, including coupled THMC simulations of pressure driven stress, strain, and MEQs coupled to geochemical and geomechanical changes in porosity, permeability, and capillary pressure.

B.4 AOR DELINEATION

To delineate the pressure front, the minimum or critical pressure necessary to reverse flow direction between the lowermost USDW and the injection zone—and thus cause fluid flow from the injection zone into the

formation matrix—must be calculated. We use the guidance provided in the May 2013 version (EPA 816-R-13-005) of the *UIC Program Class VI Well Area of Review Evaluation and Corrective Action Guidance* for the case when the deepest USDW and the storage reservoir are in hydrostatic equilibrium (Method 2). Because density in the storage formation is lower than density in the USDW, EPA's Equations 3 and 4, which come from Nicot et al. (2008) Equation 7, cannot be used. Instead, we use Nicot et al.'s Equation 9, as presented in Bandilla et al. (2012), in conjunction with 1D numerical modeling. The equation for critical pressure change (increase over original pressure) is

$$\Delta P_{crit} = gdz\left[\frac{(\lambda-\xi)}{2}dz + \rho_{ct} - \rho_w\right], \qquad \text{(Eq. 5)}$$

where

$\xi = \frac{\rho_b - \rho_w}{dz}$, $\lambda = \frac{\rho_{cb} - \rho_{ct}}{dz}$,

and g, acceleration due to gravity, 9.8 m/s^2.

The variables are illustrated in the figure below, but *dz* is used instead of *l* for the distance between the bottom of the USDW and the top of the storage formation.

FIGURE B-14. CONCEPTUAL SKETCH OF DENSITY DISTRIBUTION IN A BOREHOLE (NOT TO SCALE)

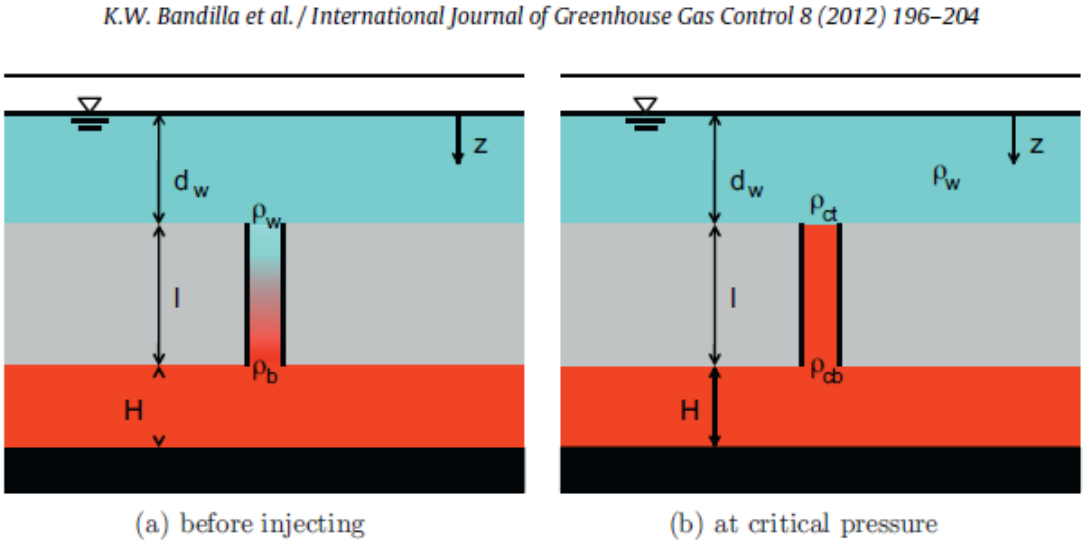

The variable ρ is fluid density, which is determined by running 1D column numerical models with TOUGH, for the scenarios in Figures B-14 (a) and 1(b) above. The 1D columns are extracted from the full model. For

B-14(a), initial hydrostatic pressure gradient, geothermal temperature gradient, and given salinity gradient are specified, and the model is allowed to come to equilibrium. Pressure, temperature, and salinity are fixed at the top of the model (the ground surface), and temperature is fixed at the base of the model (basement rock). The temperature difference between model top and bottom corresponds to a geothermal gradient of 22.7 °C/km. The initial salinity gradient is 3,349.5 ppm/km, which is estimated from local literature values. For B-14(b), the initial salinity for the entire depth interval *dz* is set to ρ_b from the Figure B-14(a) simulation, diffusion is turned off, so salinity remains nearly constant, and the simulation is allowed to come to equilibrium. Table B-5 summarizes the TOUGH simulation results.

TABLE B-5. SUMMARY OF PARAMETERS USED TO DETERMINE CRITICAL PRESSURE, TAKEN FROM 1D COLUMN MODELS

Figure 1a	Grid *z* (m)	P_0 (MPa)	T_0 (C)	Salinity (ppm)	Fluid density (kg/m^3)	Bandilla variable name
Figure 1a - normal steady state						
Tehama Bottom	-590	5.882	32.521	2,744	998.862	ρ_w
Anderson Top	-3456.6	33.82	96.456	16,658	987.274	ρ_b
Figure 1b - constant salinity between reservoir and USDW steady state						
Tehama Bottom	-590	5.886	32.522	16,468	1007.878	ρ_{ct}
Anderson Top	-3456.6	33.95	96.459	16,656	987.331	ρ_{cb}

With the above values for ρ_w, ρ_b, $\rho_{ct,}$ and $\rho_{cb,}$ and using dz = 2866.6, Equation (5) yields ΔP_{crit} = 0.127 MPa.

The AoR is delineated as the greatest extent covered by the combination of the plume and pressure fronts at the time of complete stabilization for the sequestered CO_2. The plume-based component of the AoR is defined by the boundary that encompasses the injected free-phase CO_2 with a concentration greater than 1%. The pressure-front contribution to the AoR is defined by the critical pressure calculations. Based on the preliminary modeling analyses and influenced by the closed boundary assumptions, the pressure front extends outward from IW-A1to the sealed faults to the north, west, and eastern sides of the MC project site. There is some uncertainty about the nature of the Antioch fault south of the project and on the other side of the Sacramento River. Figure B-14 shows the plume-based contribution, the pressure-front contribution to the AoR, and the resulting greatest extent covered by the combination.

FIGURE B-15. MODEL PREDICTED AOR FOR THE MC PROJECT

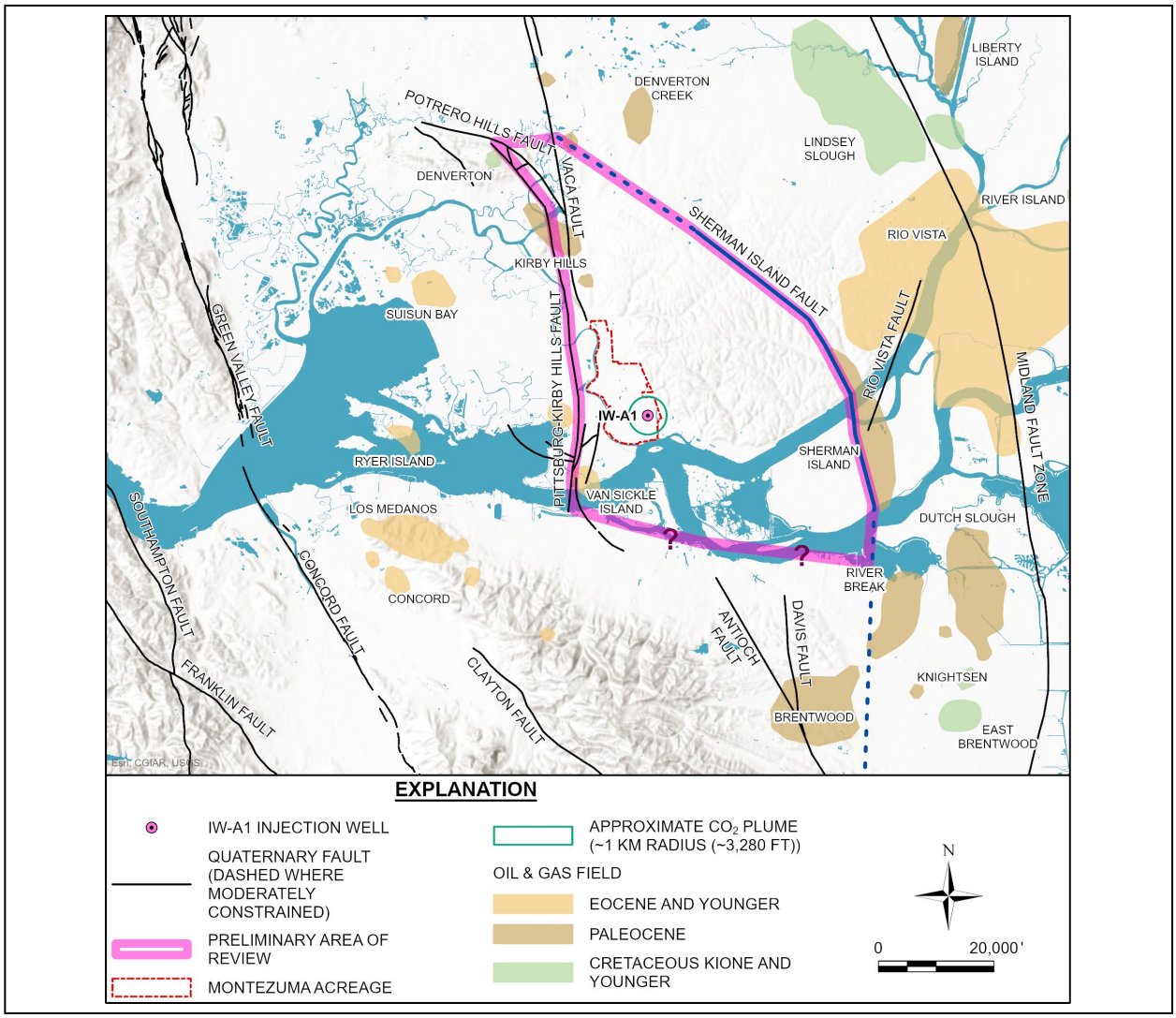

B.5 CORRECTIVE ACTION PLAN AND SCHEDULE

Figures B-16 is a map that displays the location of IW-A1, with idle/legacy oil and gas wells within the areal extent of the AoR,. These oil and gas wells are the primary type of artificial penetration of the confining units and injection zone within the AoR and immediate vicinity of the MC project site.

FIGURE B-16. AOR MAP WITH LEGACY OIL AND GAS WELLS

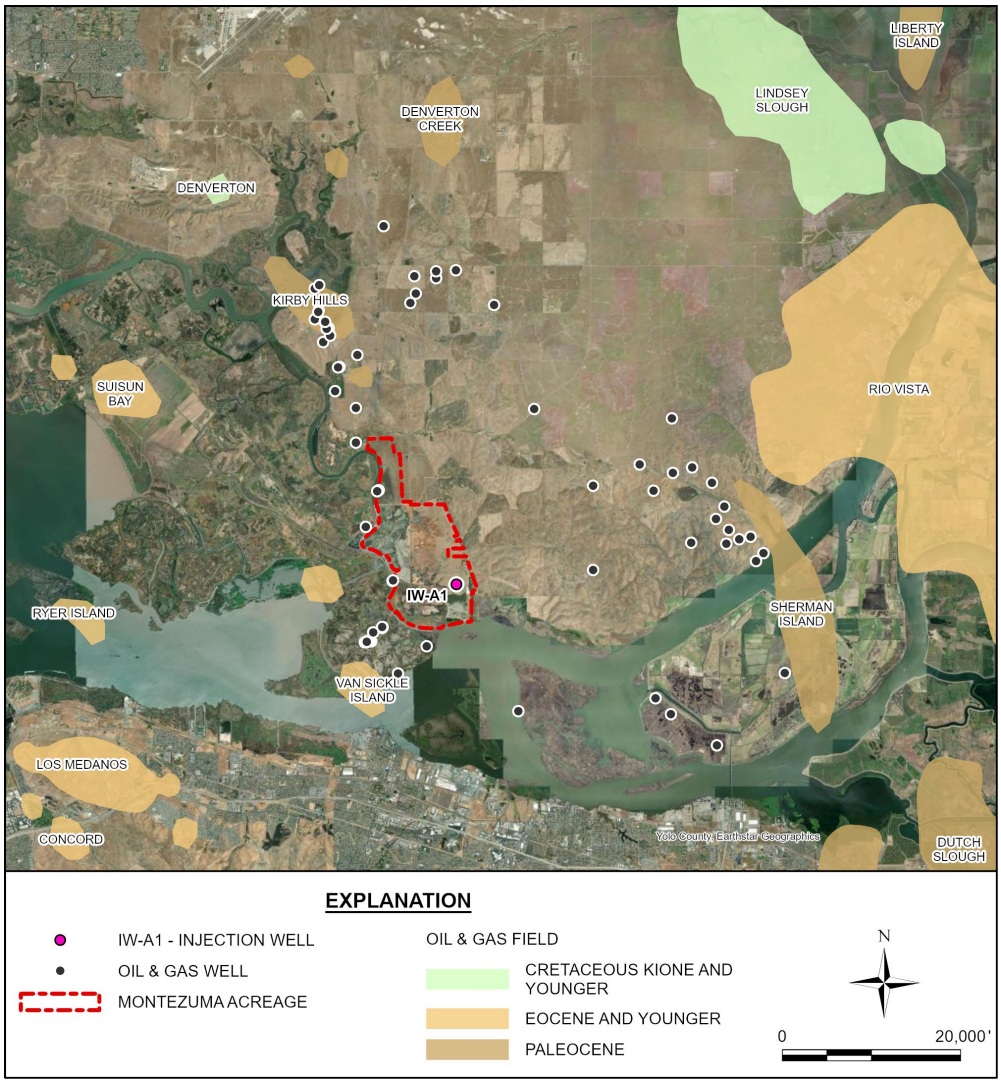

Below is a brief description of relevant research information gathered by MC for other non-well penetrations, none of which were identified as injection zone penetrations within the AoR:

- State- or US EPA-Approved Subsurface Clean-up Sites: PCC searches of the US EPA Cleanups In My Community Map and the database did not result in any candidate penetrations of the confining units or injection zone within the AoR.
- Mine and Quarries (Surface and Subsurface): The MC search of the available public records did reveal a sand dredging/mining operation permitted in Suisun Channel (Figure B-17). Other than this shallow water dredging operation, MC did not identify any other mines and quarries within the AoR or the vicinity of the project site.

FIGURE B-17. AOR MAP WITH OTHER RELEVANT IDENTIFIED SURFACE AND SUBSURFACE FEATURES

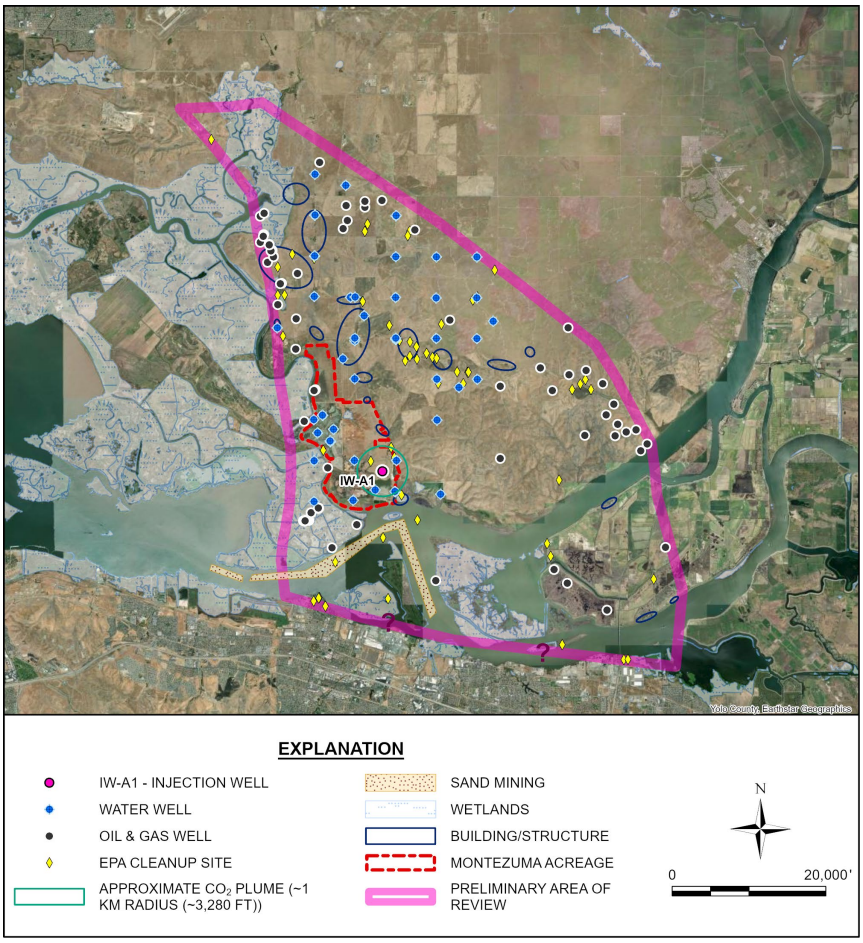

- Faults and Fractures: Multiple sealed faults are identified surrounding the project site and influence and provide structural control of the outer perimeter of the AoR, as previously described. The presence of multiple nearby gas production and storage fields supports the interpretation that these faults function as closed features. See the Site Characterization attachment to the Application Narrative for additional details and discussion of the regional geology and these features.

B.5.1. TABULATION OF WELLS WITHIN THE AOR

B.5.1.1. WELL OVERVIEW

MC searched online databases in 2023 for wells that may potentially create conduits for fluid movement out of the injection zone, and these data are summarized in Appendix B-1 for oil and gas wells and Appendix B-2 for the water wells. Below is a summary of the search findings:

- No Class I, III, IV, or VI wells were identified within the areal extent of the AoR and immediate vicinity.

- Appendix B-1 lists the search findings for one idle and six legacy oil and gas wellbores that penetrate the confining units within the AoR. Roughly 37 additional legacy wellbores that penetrate the confining zones were identified at a greater distance from, but still in the vicinity of, the MC project site. Except for the one "idle" gas production well, all of these other deep wells are reported plugged. MC plans to perform a detailed evaluation of the seven nearest and deeper wells and will also screen the more distant deep wells identified and described above.
- For the MC project site, IW-A1 and IZMW-A1 along with any other future CO_2 injection wells proposed for the project site will all be constructed to Class VI standards, thus no corrective actions are needed at this time.
- Appendix B-2 lists search findings for water wells identified within the AoR. The deepest of the wells does not exceed an 800 ft depth, and none of the water wells penetrate the multiple underlying shale units that act as confining units, providing over 9,000 ft of separation between the deepest of these wells and the Anderson Sandstone injection interval. Thus, there is no need for corrective action on any of these wells at this time.

B.5.1.2 WELLS PENETRATING THE CONFINING ZONE (UPPER MARTINEZ/MEGANOS)

Analysis of any wellbore penetrating the confining zone within the areal extent of the AoR will follow the procedures given the US EPA Guidance Document for AoR and Corrective Action (EPA 2013). Figure B-18 is a decision tree that summarizes the analysis procedure. Furthermore, procedures outlined in the guidance document will be followed for any wellbore needing to be re-entered and re-abandoned.

Figure B-18. Well Evaluation Decision Tree

From: EPA 2013

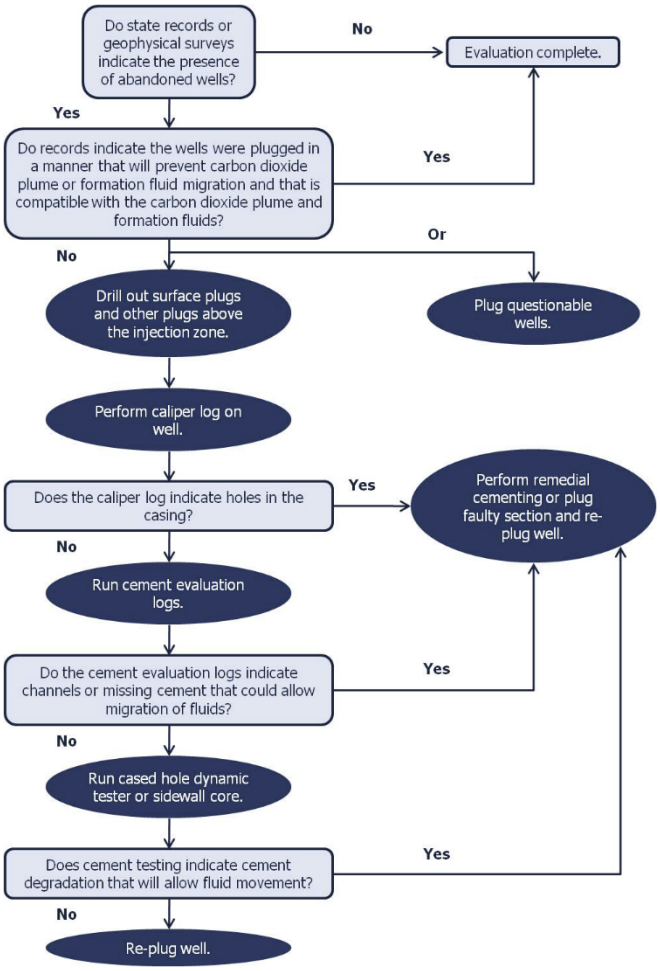

B.5.1.3 LEGACY WELLS REQUIRING CORRECTIVE ACTION

Based on the currently available information about the legacy wells in existence no corrective action is anticipated to be required. However, MC will evaluate and screen the wells identified in Appendix B-1 in more detail and has conservatively included potential corrective action for the one idle gas well and several other close deep wells within their financial responsibility plan.

B.5.2. PLAN FOR SITE ACCESS

At this time, MC does not anticipate the need to access any legacy wells for potential corrective action. However, MC is committed to obtaining such access agreements for any wells evaluated and determined to warrant corrective actions.

B.5.3. CORRECTIVE ACTION SCHEDULE

It is anticipated that any required deep well corrective actions would occur prior to the start of the Injection Period; therefore, no phased corrective actions are planned or contemplated at this time.

The scope and schedule for any future corrective actions resulting from a future AoR Re-evaluation will be developed in consultation with the US EPA UIC Program Director. Any such future corrective action will be performed after approval by the US EPA UIC Program Director.

B.6. RE-EVALUATION SCHEDULE AND CRITERIA

B.6.1. AOR RE-EVALUATION CYCLE

MC will re-evaluate the AoR at least once every 5 years (or when monitoring and operational conditions warrant) during the Injection and Post-Injection periods. For each re-evaluation, MC will:

1. Re-evaluate the AoR in the same manner specified in 40 CFR 146.84(c),
2. Identify all wells in the re-evaluated AoR that require corrective action in the same manner specified in 40 CFR 146.84(c),
3. Perform corrective action on wells requiring corrective action in the re-evaluated AoR in the same manner specified in 40 CFR 146.84(d), and
4. Submit an amended Area of Review and Corrective Action Plan or demonstrate to the Program Director through monitoring data and modeling results that no amendment to the plan is needed. Any amendment to the Area of Review and Corrective Action Plan must be approved by the Program Director, must be incorporated into the permit, and are subject to the permit modification requirements at 40 CFR 144.39 or 40 CFR 144.41 as appropriate.

B.6.2. TRIGGERS FOR AOR RE-EVALUATIONS PRIOR TO THE NEXT SCHEDULED RE-EVALUATION

Triggers that may warrant an unscheduled re-evaluation of the AoR include:

- Significant changes in site operations that may alter model predictions and the AoR delineation. Examples of such changes include but are not limited to:
  - A change in the location or number of Class VI injection wells injecting into the same injection zone
  - A change in CO_2 injection rates or pressure outside of the limits of the original permit and AoR delineation
  - A material change in the composition of the injectate

- Monitoring results for the injected CO_2 plume and/or the associated pressure front that differ significantly from computational model predictions. Examples of such differences include but are not limited to:
  - Analysis of samples from IZMW-A1 indicating CO_2 concentrations materially greater than predicted by the computational model
  - Bottom-hole pressures for IZMW-A1 materially greater than predicted by the computational model
  - Significant micro-seismic activity outside the pressure front predicted by the computational model
- Obtaining new site characterization data that may significantly change model predictions and the delineated AoR. Examples of such data include but are not limited to:
  - Newly identified potential conduits for fluid movement
  - Updated information regarding injection or confining zone extent and thickness
  - Further characterization of formation heterogeneity

MC will discuss any such events with the UIC Program Director to determine if an AoR re-evaluation is required. If an unscheduled re-evaluation is triggered, MC will perform the steps described at the beginning of this section of this Plan.

B.7 REFERENCES

Aradóttir, E.S.P., E.L. Sonnenthal, G. Björnsson, and H. Jónsson, 2012. Multidimensional reactive transport modeling of CO_2 mineral sequestration in basalts at the Hellisheidi geothermal field, Iceland. *International Journal of Greenhouse Gas Control*, 9:24-40.

Asaka, M., Holt, R.M., Bakkt, A., 2021. Rock physics model of shale: predictive aspect, Journ. Geophys. Research, Solid Earth, 126, e2021JB021993.

Bandilla, K. W., Kraemer, S. R., and Birkholzer, J. T., 2012, Using semi-analytic solutions to approximate the area of potential impact for carbon dioxide injection, International Journal of Greenhouse Gas Control, vol. 8, p. 196-204.

Birkholzer, J.T.**,** Cihan, A., Zhou, 2012, Impact-Driven Pressure Management Via Targeted Brine Extraction – Conceptual Studies of CO_2 Storage in Saline Formations, International Journal of Greenhouse Gas Control, vol. 7, p. 168-180

Brocher, T., 2004. Compressional and shear wave velocity versus depth in the San Francisco Bay Area, California: rules for USGS Bay Area velocity model 05.0.0, USGS Open file report 05-1317.

Cherven, V.B., 1983, Mesozoic through Paleogene evolution of the Sacramento basin, California, in Cherven, V.B. and Graham, S.A., eds., Geology and Sedimentology of the Southwestern Sacramento Basin and East Bay Hills: Field Trip Guidebook, Pacific Section, Society of Economic Paleontologists and Mineralogists, Los Angles, p. 21-31.

Crane, R.C., 1995, Geology of the Mt. Diablo region and East Bay hills, in Sangines, E.M., Andersen, D.E., and Buising, A.V., eds., Recent Geologic Studies in the San Francisco Bay Area: Pacific Section SEPM (Society for Sedimentary Geology), Volume 76, p. 87-114.

Division of Oil, Gas and Geothermal Resources (DOGGR), 1982a, California Oil and Gas Fields, Volume III – Northern California; Contour maps, cross sections and data sheets: California Department of Conservation, 330 p. (available from http://repository.usgin.org/category/place-keywords/california; last accessed 4/8/22)

Division of Oil, Gas, and Geothermal Resources (DOGGR) 1982b, Sherman Island gas field, *in* California Oil and Gas Fields, vol. III, Northern California: California Department of Conservation, Division of Oil and Gas, publication TR10.

Dobson, P.F., T.J. Kneafsey, S. Nakagawa, E.L. Sonnenthal, M. Voltolini, J.T. Smith, S.E. Borglin, 2021. Fracture sustainability in Enhanced Geothermal Systems: Experimental and modeling constraints. *J. Energy Resour. Technol.* 143, 100901.

Doughty, C. A., 2013, User's guide for hysteretic capillary pressure and relative permeability functionsin TOUGH2, Lawrence Berkeley National Laboratory, March.

Doughty, C., 2007, Modeling of geologic storage of carbon dioxide: comparison of non-hysteretic and hysteretic characteristic curves, Energy Conversion and Management, vol. 48(6), p. 1768-1781.

Finsterle, S., E.L. Sonnenthal, N. Spycher, 2014. Advances in subsurface modeling using the TOUGH suite of simulators. *Computers & Geosciences*, 65:2-12.

Foxall, W., Doughty, C., Lee, K.J., Nakagawa, S., Daley, T., Burton, E., Layland-Bachmann, C., Borglin, S., Freeman, K., Ajo-Franklin, J., Jordan, P., Kneafsey, T., Oldenburg, C., Ulrich, C., 2017.

Investigation of Potential Induced Seismicity Related to Geologic Carbon Dioxide Sequestration in California, Final Project Report. report to California Energy Commission, Energy Research and Development Division, CEC-500-2017-028, Sacramento, California.

Graham, S.A., Gavigan, C., McCloy, C., Hitzman, M., Ward, R., and Turner, R., 1983, Basin evolution during the change from convergent to transform continental margin: an example from the Neogene of California, in Cherven, V.B., and Graham, S.A., eds., 1983, Geology and Sedimentology of the Southwestern Sacramento Basin and East Bay Hills: Field Trip Guidebook, Pacific Section, Society of Economic Paleontologists and Mineralogists, Los Angles, p. 101-118.

Ingersoll, R. V., and Dickinson, W. R., 1981, Great Valley Group (sequence), Sacramento Valley, California, in Frizzell, V., ed., Upper Mesozoic Franciscan rocks and Great Valley sequence, central Coast ranges, California (Annual Meeting, Pacific Section SEPM field trips 1 and 4): Pacific Section, Society of Economic Paleontologists and Mineralogists, p. 1–33.

Kim, J., Sonnenthal, E.L., and Rutqvist, J., 2012. Formulation and sequential numerical algorithms of coupled fluid/heat flow and geomechanics for multiple porosity materials, *Int. J. Numer. Meth. Engng.*, 92, 425-456

Krug, E.H., Cherven, V.B., Hatten, C.W., Roth, J.C., 1992, Subsurface structure in the Montezuma Hills, southwestern Sacramento basin, in Cherven, V.B., and Edmondson, W.F., eds., Structural Geology of the Sacramento Basin: Volume MP-41, Annual Meeting, Pacific Section, Society of Economic Paleontologists and Mineralogists, p. 41-60.

Lai, M., 1999. Shale stability: drilling fluid interaction and shale strength, 1999 SPE Latin American and Caribbean Petroleum Engineering, Caracas, Venezuela.

MacKevett, N.H., 1992, The Kirby Hills fault zone, in Cherven, V.B., and Edmondson, W.F., eds., Structural Geology of the Sacramento Basin: Volume MP-41, Annual Meeting, Pacific Section, Society of Economic Paleontologists and Mineralogists, p. 61-78.

Myer, L., L. Chiaramonte, T. M. Daley, D. Wilson, W. Foxall, J. H. Beyer, 2010, Potential for Induced Seismicity Related To The Northern California CO_2 Reduction Project Pilot Test, Solano County, California, LLNL-TR-435831 June 15.

Nicot, J. P., Oldenburg, C. M., Brynt, S. L., and Hovorka, S. D., 2008, Pressure perturbation from geologic carbon sequestration: Area-of-review boundaries and borehole leakage driving forces. Energy Procedia.

Oldenburg, Curtis M. and Preston D. Jordan, 2017, Long-Term Viability of Underground Natural Gas Storage in California, An Independent Review of Scientific and Technical Information, California Council on Science and Technology December.

Pan, L., Spycher, N., Doughty, C., and Pruess, K. 2015. ECO2N V2.0: A TOUGH2 fluid property module for mixtures of water, NaCl, and CO_2. Earth Sciences Division, Lawrence Berkeley National Laboratory, University of California, Berkeley. LBNL-6930E. February.

Pasquini, D.E., and Milligan, H.L., 1967, Correlation Section 15, Sacramento Valley, Suisun Bay to Lodi: Pacific Section, American Association of Petroleum Geologists.

Peaceman, D. W., 1977, Interpretation of well-block pressures in numerical reservoir simulation, SPE 6893, 52nd Annual Fall Technical Conference and Exhibition, Denver, 1977.

Pratt, H. R., W. A. Hustrulid, and D. E. Stephenson, 1978, Earthquake Damage to Underground Facilities, Environmental Transport Division, November.

Pruess, K., Oldenburg, C., and Moridis, G., 2012, TOUGH2 User's Guide, Version 2, Earth Sciences Division, Lawrence Berkeley National Laboratory, University of California, Berkeley. LBNL-43134. September

Pruess, K., Garca, J., Kovscek, T., Oldenburg, T. C., Rutqvist, J., Steefel, C., & Xu, T., 2004, Code intercomparison builds confidence in numerical simulation models for geologic disposal of CO_2, Energy, vol. 29(9-10), p. 1431-1444.

Pruess, K., Oldenburg, C., and Moridis, G., 2011, TOUGH2 User's Guide.

Pruess, K., and Spycher, N., 2007, ECO2N – A fluid property module for the TOUGH2 code for studies of CO_2 storage in saline aquifers, Energy Conversion and Management, vol. 48, p. 1761-1767.

Smith, J.T., Sonnenthal, E.L., and Cladouhos, T., 2015. Thermal-Hydrological-Mechanical Modelling of Shear Stimulation at Newberry Volcano, Oregon. *Proceedings of 49th US Rock Mechanics/Geomechanics Symposium*, American Rock Mechanics Association, ARMA 15-0680.

Sonnenthal, E., N. Spycher, T. Xu, and L. Zheng, 2021. TOUGHREACT V4.12-OMP and TReactMech V1.0 Geochemical and Reactive-Transport User Guide. LBNL Report 2001410. https://tough.lbl.gov/software/toughreact.

Sonnenthal, E., W. Pettitt, T. Smith, A. Riahi, D. Siler, E. Majer, P. Dobson, B. Ayling, B. Damjanac, 2018. Continuum thermal-hydrological-mechanical modeling of the Fallon FORGE Site, GRC Transactions, 42, 10 p.

Spycher, N., and Pruess, K., 2005, Carbon dioxide-water mixtures in geologic sequestration of carbon dioxide. II. Partitioning in chloride brines at 12-100 degrees Celsius and up to 600 bar. Geochemical et Cosmochimica Acta, vol. 69, p. 3309-3320.

Segall, P. (1989), Earthquakes triggered by fluid extraction, Geology, 17, 942–946.

Sloan, D., Schwartz, D., and Unruh, J., Regional Geology of Mount Diablo, California: Its Tectonic Evolution on the North American Plate Boundary: Geological Society of America Memoir 217, p. 179-200.

Suckale, J. (2009), Induced seismicity in hydrocarbon fields, Adv. Geophys., 51, 55–106.

Sullivan, R., Sullivan, M.D., Dedmon, P., and Edwards, S.W., 2021a, The occurrence and mining of coal and sand deposits in the Middle Eocene Domengine Formation of the Mount Diablo Coalfield, California, in Sullivan, R., Sloan, D., Schwartz, D., and Unruh, J., Regional Geology of Mount Diablo, California: Its Tectonic Evolution on the North American Plate Boundary: Geological Society of America Memoir 217, p. 65-95.

Sullivan, R., Sullivan, M.D., Edwards, S.W., Sarna-Wojicicki, A., Hackworth, R.A., Deino, A.L., 2021b, The mid-Cenozoic succession on the northeast limb of Mount Diablo anticline, California-a stratigraphic record of tectonic events in the forearc basin, in Sullivan, R., Sloan, D., Schwartz, D., and Unruh, J., Regional Geology of Mount Diablo, California: Its Tectonic Evolution on the North American Plate Boundary: Geological Society of America Memoir 217, p. 269-303.

United States Environmental Protection Agency (EPA). 2013. UIC Program Class VI Well Area of Review Evaluation and Corrective Action Guidance. EPA 816-R-13-005.

Unruh, J.R., and Hector, S.T., 1999, Subsurface Characterization of the Potrero-Ryer Island Thrust System, Western Sacramento-San Joaquin Delta, Northern California: Final Technical Report submitted to the U.S. Geological Survey, National Earthquake Hazards Reduction Program award number 1434-HQ-96-GR-02724, 32 p.

Unruh, J., Hitchcock, C., Blake, K., and Hector, S., 2016, Characterization of the Southern Midland Fault in the Sacramento-San Joaquin Delta, in Ferriz, H. and Anderson, R., eds., Applied Geology in California: Association of Engineering Geologists, Special Publication 26, p. 757-776.

Unruh, J., 2021, Upper plate deformation during blueschist exhumation, ancestral western California forearc basin, from stratigraphic and structural relationships at Mount Diablo and in the Rio Vista Basin, in Sullivan, R.,

Walsh, F.R., and Zoback, M.D., 2015, Oklahoma's recent earthquakes and saltwater disposal: Science Advances, v. 1, e1500195, doi:10.1126 /sciadv.1500195.

Xu, T., N. Spycher, E. Sonnenthal, G. Zhang, L. Zheng, and K. Pruess, 2011. TOUGHREACT Version 2.0: A simulator for subsurface reactive transport under non-isothermal multiphase flow conditions. Computers & Geosciences, 37:763–774.

Zhai, G., M. Shirzaei, and M. Manga (2021) Widespread deep seismicity in the Delaware Basin, Texas, is mainly driven by shallow wastewater injection, PNAS, vol. 118, e2102338118.

APPENDIX B-1

OIL AND GAS WELLS

APPENDIX B-1. OIL & LEGACY WELLS

O&G well locations identified warranting detailed evaluation for future corrective actions - Seven (7)

TOWNSHIP	RANGE	SECTION	County	Field	Latitude	Longitude	API No.	Well Name	Well Number	Year Drilled	Yr Abandon	Original Hole TD	RD1 T.D.	RD2 T.D.	CalGEM STATUS	CalGEM Type	SURF. CSG. SIZE	SETTING DEPTH	2nd CSG. STRING	SETTING DEPTH	3rd CSG. STRING	SETTING DEPTH	API No.	Anderson Top	Anderson Base	Anderson Thickness
T2N	R1E	8	Contra Costa	Wildcat	38.035677	-121.8813	01300275	Browns Island Unit	1	1964	1964	10006	12100		PLUGGED	DRY HOLE	9-5/8"	1506					01300275			
T3N	R1E	6	Solano	Wildcat	38.083044	-121.919661	09520965	McDougal Livestock	1	1993	1993	7142			PLUGGED	DRY HOLE	10-3/4"	1500	7"	5389			09520965	8415		
T3N	R1E	8	Solano		38.114487	-121.888824	09520674	Swepi-Hershey State	1-8	1984	1984	9328			PLUGGED	DRY HOLE	20"	518	13.375	2038	9.625"	6977	09520674	9288		
T3N	R1E	8	Solano	Wildcat	38.114182	-121.889433	09520724	McDougal	2-8	1985	1985	12191			PLUGGED	DRY HOLE	13-3/8"	722	9-5/8"	7173			09520724	9892	10500	608
T3N	R1E	19	Solano	Wildcat	38.0815029	-121.903105	09500420	Dow Chemical Co.-Ward	1	1953	1953	8966			PLUGGED	DRY HOLE	11-3/4"	1002	7"	7520			09500420	8611	8774	163
T3N	R1E	20	Solano	Van Sickle Island Gas Field	38.0865702	-121.8833583	09521296	Roaring River	20-4	2008	idle	8201	8500	7858	IDLE	DRY GAS	10-3/4"	1531	7"	7855			09521296			
T3N	R1W	24	Solano	Honker Gas Field	38.082673	-121.918898	09520206	Standard - King	1	1976	1976	11070			PLUGGED	DRY HOLE	13-3/8"	1596	9-5/8"	7950			09520206	9160	10051	891

O&G well locations identified warranting further evaluation and potentially may require future corrective actions - thirty seven (37)

TOWNSHIP	RANGE	SECTION	County	Field	Latitude	Longitude	API No.	Well Name	Well Number	Year Drilled	Yr Abandon	Original Hole TD	RD1 T.D.	RD2 T.D.	CalGEM STATUS	CalGEM Type	SURF. CSG. SIZE	SETTING DEPTH	2nd CSG. STRING	SETTING DEPTH	3rd CSG. STRING	SETTING DEPTH	API No.	Anderson Top	Anderson Base	Anderson Thickness
T2N	R2E	5	Sacramento	Wildcat	38.050167	-121.7811331	06720166	Lower Sherman Island	1	1980	1981	8595			PLUGGED	DRY HOLE	8-5/8"	904	8-5/8"	904			06720166	8420		
T2N	R2E	5	Sacramento		38.05101	-121.78112	06720166	Lower Sherman Island	1	1980	1980	8595			PLUGGED	DRY HOLE	8.625"	904					06720166	8420		
T2N	R2E	5	Sacramento	Wildcat	38.0453236	-121.7751905	06700295	Signal-R.I.L. Co.	1	1965	1965	8835			PLUGGED	DRY HOLE	9-5/8"	800	9-5/8"	800			06700295	8078	8680	602
T3N	R2E	5	Solano	Wildcat	38.1364346	-121.7744585	09520430	Anderson	1-5	1980	1980	14269			PLUGGED	DRY HOLE	13-3/8"	1499	7-5/8"	13183			09520430	7825	8189	364
T3N	R2E	8	Solano	Sherman Island Gas Field	38.1222444	-121.7870538	09520450	Neil	1	1981	1981	9600			PLUGGED	DRY HOLE	9-5/8"	1022					09520450	8035	8550	515
T3N	R2E	8	Solano	Sherman Island Gas Field	38.11967	-121.774135	09500426	Dozier-Pressley	1	1965	1965	10503			PLUGGED	DRY HOLE	9-5/8"	1009					09500426	7420	7828	408
T3N	R2E	9	Solano	Sherman Island Gas Field	38.116502	-121.75894	09520702	Dozier & Pressley	2-9	1984	1984	7162			PLUGGED	DRY HOLE	8-5/8"	910					09520702	6685	7097	412
T3N	R2E	9	Solano	Sherman Island Gas Field	38.1212442	-121.766501	09520697	Dozier & Pressley	1-9	1984	1984	7307			PLUGGED	DRY HOLE	8-5/8"	907					09520697	6840	7261	421
T3N	R2E	15	Solano	Sherman Island Gas Field	38.099136	-121.748396	09520321	Dozier & Pressley Co.	4	1976	1976	6707			PLUGGED	DRY HOLE	9-5/8"	736					09520321	6400		
T3N	R2E	15	Solano	Sherman Island Gas Field	38.0677315	-121.8935222	09520124	Dozier & Pressley	2	1970	2015	6800			PLUGGED	INJECTION	8-5/8"	718	4-1/2"	6541			09520124	6352		
T3N	R2E	15	Solano	Sherman Island Gas Field	38.098188	-121.7388722	09520093	Dozier & Pressley Co.	1	1969	1981	7518			PLUGGED	GAS	9-5/8"	775	2-7/8"	6564			09520093	6500	6680	180
T3N	R2E	15	Solano	Sherman Island Gas Field	38.107177	-121.740789	09520239	D. P. M. Unit	1	1974	1974	8132			PLUGGED	DRY HOLE	8-5/8"	1011					09520239	7220		
T3N	R2E	16	Solano	Sherman Island Gas Field	38.109213	-121.753986	09520127	Dozier-Pressley Co.	3	1970	1980	6950			PLUGGED	GAS	8-5/8"	720	4-1/2"	6950			09520127	6805		
T3N	R2E	16	Solano	Sherman Island Gas Field	38.102027	-121.75228	09520125	Dozier-Pressley	2	1970	1971	8020			PLUGGED	GAS	8-5/8"	780	5-1/2"	4930			09520125	6885	7059	174
T3N	R2E	16	Solano	Sherman Island Gas Field	38.097797	-121.753318	09500427	Dozier-Pressley	1	1946	1946	8025			PLUGGED	DRY HOLE	9-5/8"	507					09500427	6775	7150	375
T3N	R2E	16	Solano	Sherman Island Gas Field	38.0981119	-121.7670576	09520878	Dozier-Pressley	1	1990	1990	8500			PLUGGED	DRY HOLE	8-5/8"	854					09520878	7510	8000	490
T3N	R2E	22	Solano	Sherman Island Gas Field	38.0924256	-121.7418121	09521011	West Dozier	1	1995	1996	6700	6520		PLUGGED	GAS	8-5/8"	697					09521011	6325		
T3N	R2E	22	Solano	Sherman Island Gas Field	38.094876	-121.73889	09520154	Decker Island Unit	5	1971	1971	7750	6874		PLUGGED	GAS	8-5/8"	730					09520154			
T4N	R1E	7	Solano	Wildcat	38.19576	-121.886818	09520963	Gunn	1	1993	1993	9310			PLUGGED	DRY HOLE	8-5/8"	1070					09520963	7260	8348	1088
T4N	R1E	9	Solano	Wildcat	38.199701	-121.869443	09521049	Mayhood	1	1998	1998	10298			PLUGGED	DRY HOLE	9-5/8"	1472					09521049	8450	9290	840
T4N	R1E	9	Solano	Kirby Hill Gas Field	38.200498	-121.865224	09521048	Petersen	1	1999	1999	10371			PLUGGED	GAS	9-5/8"	1107	5-1/2"	6223	2-7/8"	10340	09521048	8555	9310	755
T4N	R1E	12	Solano	Wildcat	38.200589	-121.821493	09520793	Hagan	2-12	1987	1987	10085			PLUGGED	DRY HOLE	10-3/4"	2080					09520793	8507	8816	309
T4N	R1E	15	Solano	Wildcat	38.1858609	-121.852744	09520812	Shiloh	1-15	1987	1988	10,700			PLUGGED	DRY HOLE	10-3/4"	2097					09520812	8974	9515	541
T4N	R1E	21	Solano	Wildcat	38.17964	-121.866248	09500005	Turner	1	1966	1967	10449			PLUGGED	DRY HOLE	10-3/4"	1025					09500005	9150	9748	598
T4N	R1E	21	Solano	Wildcat	38.18028	-121.874746	09520080	Sumpf-Williams-O'Brien	1	1969	1969	10600			PLUGGED	DRY HOLE	11-3/4"	507	8-5/8"	6773			09520080	8866	9444	578
T4N	R1E	21	Solano	Wildcat	38.172033	-121.876289	09521120	R. W. Blacklock	2-21	2001	2003	11544			PLUGGED	DRY GAS	13-3/8"	833	9-5/8"	7953	4-1/2"	11226	09521120	8924	9588	664
T4N	R1E	21	Solano	Wildcat	38.18181	-121.866255	09520017	Sumpf-Williams-Turner	2	1967	1968	12216			PLUGGED	DRY HOLE	10-3/4"	2809	7"	8747	4-1/2"	12193	09520017	9155	9598	443
T4N	R1E	22	Solano	Wildcat	38.182131	-121.858574	09520750	McGraugh	1-22	1986	1989	10,595			PLUGGED	DRY GAS	10-3/4"	2026	5-1/2"	10876			09520750	9186	9745	559
T4N	R1E	24	Solano	Wildcat	38.183203	-121.807013	09520449	Hagen	1	1984	1984	9,503	9249		PLUGGED	DRY HOLE	9-5/8"	1039	2-7/8"	9316			09520449	8155	8671	516
T4N	R1E	31	Solano	Kirby Hill Gas Field	38.144964	-121.905745	09500079	Fontana Farms	4	1945		5800			PLUGGED	GAS	11-3/4"	568	7"	3030			09500079	5488		
T4N	R1E	31	Solano	Kirby Hill Gas	38.152496	-121.904076	09500063	Standard-Kirby Community	8R	1963	1963	6421			PLUGGED	DRY HOLE	13.375"	302	7"	1062			09500063	5314	5979	665
T4N	R2E	18	Solano	Wildcat	38.19644	-121.797704	09520068	U.S.A.A.R. Blodgett	1	1968	1968	10,601			PLUGGED	DRY HOLE	10-3/4"	1992					09520068	7675		
T4N	R2E	19	Solano	Wildcat	38.1821312	-121.7971944	09520215	Sage-Phillips-Sumpf-Kroutch	1	1973	1973	11,510			PLUGGED	DRY HOLE	10-3/4"	1516	7"	10999			09520215	7861	8300	439
T4N	R2E	20	Solano	Wildcat	38.173602	-121.781646	09500435	Montezuma Community	1	1944	1944	7,400			PLUGGED	DRY HOLE	11-3/4"	670					09500435	7345		
T4N	R2E	29	Solano	Wildcat	38.154702	-121.78719	09520976	Hierlihy Estate	1	1994	1994	9000			PLUGGED	DRY HOLE	8-5/8"	944					09520976	7852		
T4N	R2E	29	Solano	Wildcat	38.1668533	-121.7816679	09520011	S.A.A. Unit 1	1	1967	1967	11645			PLUGGED	DRY HOLE	10-3/4"	1153	7"	6684			09520011	7178	7540	362
T4N	R2E	30	Solano	Wildcat	38.166082	-121.798193	09520489	Hamilton Ranch	1	1982	1982	9,196			PLUGGED	DRY HOLE	9-5/8"	1003					09520489	8045	8411	366
T4N	R2E	32	Solano	Wildcat	38.146737	-121.785892	09520995	Mayhood	32-1D	1995	1995	11440			PLUGGED	DRY HOLE	9-5/8"	1439					09520995	8050		

APPENDIX B-2

WATER WELLS

APPENDIX B-2. WATER WELLS

OBJECTID	Section	Township	Range	WCR_No_	Latitude	Longitude	Date_Work_Ended	Total_Depth	Top_of	Bottom_of	Casing_Size	Planned_Use	Drilling_Company
DOMESTIC WELLS													
1				WCR1994-000929	38.13243	-121.85243	1994-04-03 00:00:00	120			5"	Domestic	Vaca Drilling Co.
3	3	T3N	R1E	WCR1991-004184	38.132778	-121.8525	1991-09-07 00:00:00	220	25	220	5"	Domestic	Vaca Drilling Co.
5				WCR2010-001159	38.13289	-121.85243		400	360	400	6"	Domestic	Woodward Drilling Co.
6	4	T3N	R1E	WCR1982-001391	38.13296	-121.87098	1982-08-12 00:00:00	100				Domestic	Vaca Drilling Co.
7	1	T3N	R1E	WCR2011-005762	38.138889	-121.808333	2011-11-17 00:00:00	320	270	310	6"	Domestic	DeJesus Pump Well Drilling
21	26	T3N	R1E	WCR1980-001076	38.077170	-121.832290	1980-12-16 00:00:00	100			5"	Domestic	Vaca Drilling Co.
22				WCR1982-001399	38.078056	-121.852778	1982-09-27 00:00:00	100			5"	Domestic	Vaca Drilling Co.
25	20	T3N	R1E	WCR1986-004919	38.089167	-121.889444	1986-06-23 00:00:00	101			5"	Domestic	Vaca Drilling Co.
32				WCR1954-000264	38.089220	-121.852230	not listed	210	70	210	6"	Domestic	Vaca Drilling Co.
43	12	T3N	R1E	WCR1975-000465	38.118160	-121.815620		120	40	120	5"	Domestic	Vaca Drilling Co.
44	11	T3N	R1E	WCR1989-010443	38.118250	-121.833910	1989-07-17 00:00:00	200			5"	Domestic	Vaca Drilling Co.
45				WCR1975-00464	38.118390	-121.871080	1975-08-27 00:00:00	221	25	220		Domestic	Vaca Drilling Co.
47				WCR1997-005860	38.132060	-121.870980	1997-10-23 00:00:00	240	78	254	5"	Domestic	Vaca Drilling Co.
48	2	T3N	R1E	WCR0047180	38.132778	-121.834167	1981-10-14 00:00:00	149			6.625"	Domestic	Vaca Drilling Co.
49				WCR1988-007782	38.132778	-121.834167	1988-09-20 00:00:00	260			6"	Domestic	Vaca Drilling Co.
51				WCR2010-001149	38.132960	-121.870980	2010-10-27 00:00:00	295			6"	Domestic	A&A Gross Drilling
52				WCR1991-000769	38.132960	-121.870980	1991-05-22 00:00:00	65			6"	Domestic	Carter Water Well Drilling
53				WCR1997-005863	38.132960	-121.870980	1997-09-22 00:00:00	200	60	200	5"	Domestic	Vaca Drilling Co.
54				WCR1956-000526	38.132960	-121.870980	1956-06-24 00:00:00	60	40	60	6"	Domestic	Vaca Drilling Co.
33	21	T3N	R1E	WCR1954-000265	38.089250	-121.871240						Domestic	Vaca Drilling Co.
57	35	T4N	R1E	WCR1997-005866	38.147222	-121.834167	1997-10-23 00:00:00	260			5"	Domestic Water Supply	Vaca Drilling Co.
58	36	T4N	R1E	WCR2007-001716	38.147260	-121.815800	2007-10-24 00:00:00	200	160	200	5"	Domestic Water Supply	Vaca Drilling Co.
59	36	T4N	R1E	WCR2007-001717	38.147260	-121.815800	2007-10-29 00:00:00	220	40	220	5"	Domestic Water Supply	Vaca Drilling Co.
60	36	T4N	R1E	WCR1951-000551	38.147260	-121.815800		28	21	28	6"	Domestic Water Supply	Owner of Well
63	33	T4N	R1E	WCR2008-001635	38.147590	-121.870840		300	160	300	6"	Domestic Water Supply	A&A Gross Drilling
65	25	T4N	R1E	WCR1977-002210	38.161820	-121.815670	1977-11-03 00:00:00	103	80	100	5"	Domestic Water Supply	Vaca Drilling Co.
66	25	T4N	R1E	WCR1997-005864	38.161820	-121.815670	1997-09-28 00:00:00	260	120	260	5"	Domestic Water Supply	Vaca Drilling Co.
67	26	T4N	R1E	WCR1982-002019	38.161900	-121.834010	1982-01-01 00:00:00	174			9"	Domestic Water Supply	Seebeck
68	26	T4N	R1E	WCR1985-000470	38.161900	-121.834010	1985-11-04 00:00:00	181			5"	Domestic Water Supply	Vaca Drilling Co.
71	29	T4N	R1E	WCR1985-000454	38.162360	-121.889100	1985-09-22 00:00:00	101			6"	Domestic Water Supply	Vaca Drilling Co.
72	29	T4N	R1E	WCR1999-005850	38.162360	-121.889100	1999-10-19 00:00:00	120			5"	Domestic Water Supply	Vaca Drilling Co.
73	29	T4N	R1E	WCR1974-00406	38.162360	-121.889100	1974-07-22 00:00:00	121	50	120	6"	Domestic Water Supply	Vaca Drilling Co.
74	29	T4N	R1E	WCR2006-000682	38.162360	-121.889100		150	30	150	5"	Domestic Water Supply	Vaca Drilling Co.
75	29	T4N	R1E	WCR1990-000913	38.162360	-121.889100	1990-06-26 00:00:00	120			6"	Domestic Water Supply	Carter Water Well Drilling Service
77	22	T4N	R1E	WCR2001-003995	38.176580	-121.852250	2001-05-16 00:00:00	260	100	260	5"	Domestic Water Supply	Vaca Drilling Co.
78	22	T4N	R1E	WCR1978-000121	38.176667	-121.852222	1978-10-13 00:00:00	247	70	240		Domestic Water Supply	Vaca Drilling Co.
79	20	T4N	R1E	WCR2006-000681	38.176820	-121.88900	2006-06-18 00:00:00	280	55	280	5"	Domestic Water Supply	Vaca Drilling Co.
80	20	T4N	R1E	WCR1991-004174	38.176820	-121.889000	1991-06-20 00:00:00	140	100	140	5"	Domestic Water Supply	Vaca Drilling Co.

APPENDIX B-2. WATER WELLS

OBJECTID	Section	Township	Range	WCR_No_	Latitude	Longitude	Date_Work_Ended	Total_Depth	Top_of	Bottom_of	Casing_Size	Planned_Use	Drilling_Company
82	20	T4N	R1E	WCR1986-004937	38.176944	-121.888889	1986-08-07 00:00:00				5"	Domestic Water Supply	Vaca Drilling Co.
83	20	T4N	R1E	WCR1974-000407	38.176944	-121.888889	1974-07-23 00:00:00	142	30	140	6"	Domestic Water Supply	Vaca Drilling Co.
85	17	T4N	R1E	WCR1973-000801	38.191490	-121.888930	1973-04-22 00:00:00	121	60	110	5"	Domestic Water Supply	Vaca Drilling Co.
86	17	T4N	R1E	WCR1957-000159	38.191490	-121.888930	1957-01-30 00:00:00	60	31	59	6"	Domestic Water Supply	H. O. Krossa
61	34	T4N	R1E	WCR1989-011955	38.147460	-121.852520	1989-11-03 00:00:00	140			5"	Water Supply	Vaca Drilling Co.
69	27	T4N	R1E	WCR1989-011954	38.161990	-121.852370	1989-11-02 00:00:00	180			5"	Water Supply	Vaca Drilling Co.
81	20	T4N	R1E	WCR1995-003844	38.176820	-121.889000	1995-06-25 00:00:00	140	40	140	5"	Water Supply	Vaca Drilling Co.
38	14	T3N	R1E	WCR1981-003162	38.103611	-121.833889	1981-06-14 00:00:00	78			7"	Water Supply	Seebeck Drilling
INDUSTRIAL/AGRICULTURAL WELLS													
9	28	T3N	R1E	WCR2002-00456	38.075040	-121.871840	2002-06-06 00:00:00	80	24	64	10"	Industrial Water Supply	Gregg Drilling and Testing
11				WCR2002-00460	38.075040	-121.871840	2002-06-06 00:00:00	80	20	50	10"	Industrial Water Supply	Gregg Drilling and Testing
12				WCR2002-00458	38.075040	-121.871840	2002-06-06 00:00:00	80	20	70	10"	Industrial Water Supply	Gregg Drilling and Testing
13				WCR2002-00457	38.075040	-121.871840	2002-06-06 00:00:00	80	26	66	10"	Industrial Water Supply	Gregg Drilling and Testing
14				WCR2002-00459	38.075040	-121.871840	2002-06-06 00:00:00	50	20	50	10"	Industrial Water Supply	Gregg Drilling and Testing
16				WCR2002-000461	38.075040	-121.871840	2002-06-06 00:00:00	80	20	50	10"	Industrial Water Supply	Gregg Drilling and Testing
17				WCR2002-000463	38.075040	-121.871840	2002-06-06 00:00:00	53	15	20	10"	Industrial Water Supply	Gregg Drilling and Testing
18				WCR2002-000452	38.075040	-121.871840	2002-06-06 00:00:00	78	34	44	10"	Industrial Water Supply	Gregg Drilling and Testing
19				WCR2002-000462	38.075040	-121.871840	2002-06-06 00:00:00	50	18	50	10"	Industrial Water Supply	Gregg Drilling and Testing
20				WCR2002-000453	38.075040	-121.871840	2002-06-06 00:00:00	70	34	64	10"	Industrial Water Supply	Gregg Drilling and Testing
42				WCR2012-00374	38.115278	-121.823889		200	60	200	5"	Agricultural & Irrigation	Pacific Coast Well and Pump, inc.
30				WCR1057-000039	38.089220	-121.852230	1957-01-15 00:00:00	773	100	773	13"	Irrigation-Agriculture	Eaton Drillng Co.
50				WCR1981-003176	38.132800	-121.834080	1981-10-14 00:00:00	150			9"	Irrigation-Agriculture	Seebeck Drilling
PUBLIC SUPPLY WELLS													
23	27	T3N	R1E	WCR1990-004026	38.078170	-121.852940	1990-03-28 00:00:00	300	240	300	6"	Public Water Supply	Ronald L. Clark